2D Covalent Organic Frameworks for Biomedical Applications

Sukanya Bhunia, Kaivalya A. Deo, and Akhilesh K. Gaharwar*

Covalent organic frameworks (COFs) are an emerging class of organic crystalline polymers with well-defined molecular geometry and tunable porosity. COFs are formed via reversible condensation of lightweight molecular building blocks, which dictate its geometry in two or three dimensions. Among COFs, 2D COFs have garnered special attention due to their unique structure composed of two-dimensionally extended organic sheets stacked in layers generating periodic columnar π-arrays, functional pore space, and their ease of synthesis. These unique features in combination with their low density, high crystallinity, large surface area, and biodegradability have made them an excellent candidate for a plethora of applications ranging from energy to biomedical sciences. In this article, the evolution of 2D COFs is briefly discussed in terms of different types of chemical linkages, synthetic strategies of bulk and nanoscale 2D COFs, and their tunability from a biomedical perspective. Next, the biomedical applications of 2D COFs specifically for drug delivery, phototherapy, biosensing, bioimaging, biocatalysis, and antibacterial activity are summarized. In addition, current challenges and emerging approaches in designing 2D COFs for advanced biomedical applications are discussed.

1. Introduction

Porous polymeric materials with highly ordered structure and tunable porosity are emerging class of materials for diverse applications in gas storage, separation, and catalysis.[1] A wide range of porous polymeric materials have been developed in the past decades including porous organic materials (POMs) (e.g., conjugated microporous polymers (CMPs), polymers with intrinsic microporosity (PIMs), hyper-crosslinked polymers (HCPs), etc.), porous inorganic materials (e.g., mesoporous

silica, titanium dioxide, etc.) as well as porous hybrid materials (organosilica), etc., offering distinct ranges of porosity including micro-(<2 nm), meso-(2–50 nm), macro-(>50 nm) length scale. However, it has long been a challenge to develop highly ordered porous materials where precise and simultaneous control over pore geometries and chemical functionalities is possible, which can be leveraged to tailor the functions for designed applications. With the recent advances in "reticular chemistry" it has been possible to combine molecular building units to build up a programmed robust extended network structure with periodic porosity. Metal-organic frameworks (MOFs), the coordination polymers that are composed of organic building blocks and metal ions connected via coordination bonds, are the first member[2] of such modular porous crystalline materials, which have created a benchmark in hydrocarbon separation.[3] Efforts to replace the metal ions with pure organic building blocks, while maintaining the crystalline framework structure and tunability have led to a new generation of sister material namely, covalent organic frameworks (COF).[4]

COFs are crystalline porous organic polymers, which are gaining enormous interest lately[5] because of their tunable pores,[6] permanent porosity,[7] low density,[1b] high specific surface area,[8] and high thermal stability.[9] Although initially COFs have been explored for gas storage and separation,[10] the function-led modular nature of the material has opened up several other new potential applications including catalysis,[11] optoelectronics,[12] as well as in drug delivery[13] and different other aspects of biomedical sciences.[14] COFs differ from other classes of covalent organic polymers mainly in terms of structural regularity, ordered and tunable porosity and functionalization.[15] Unlike the classical amorphous polymeric porous organic materials (POMs) which are connected via irreversible covalent bond,[16] COFs are formed by reversible condensation of the molecular building block,[17] which render crystallinity as well as biodegradability in such materials. Importantly, along with the scope of surface functionalization, the abundant ordered pores in COFs can be tuned in terms of size, shape, and function,[18] which offers ample scope to tailor such porous materials for a particular biomedical purpose. Additionally, the uniform pore size distribution in crystalline COFs may offer more predictable drug release behavior[19] compared to the amorphous POMs with irregular porosity. Furthermore, often being comprised of lightweight atoms, such as H, C, B, N, and O, COFs possess better scope of biocompatibility compared to some of MOFs[20] as the former lack potentially hazardous metal part.

Dr. S. Bhunia, K. A. Deo, Prof. A. K. Gaharwar
Biomedical Engineering
College of Engineering
Texas A&M University
College Station, TX 77843, USA
E-mail: gaharwar@tamu.edu

Prof. A. K. Gaharwar
Material Science and Engineering
College of Engineering
Texas A&M University
College Station, TX 77843, USA

Prof. A. K. Gaharwar
Center for Remote Health Technologies and Systems
Texas A&M University
College Station, TX 77843, USA

2002046 (1 of 27)

COF was first reported in 2005[4] and since then several other COFs are designed and synthesized by exploring different types of linkages & building blocks and synthetic strategies to achieve different physicochemical properties, tunable porosity, cost-effective synthesis, and targeting property. Mostly, 2D and a few 3D COFs[10a,21] are reported so far because of the ease of synthesis of 2D COFs (**Figure 1**). There are no significant differences between 2D or 3D COFs except the bonding connectivity of the building blocks.[22] The 3D COFs possess higher specific surface area, which makes them suitable for gas storage applications.[23] On the other hand, in 2D COFs the two-dimensionally extended organic sheets stacked in layers generates periodic columnar π-arrays, which make them exceptional candidate for photoelectrical property[12c] enabling their biomedical exploration beyond drug carrier into phototherapy and theragnostic of cancer. Furthermore, a great deal of interest is currently being employed in their morphological control particularly in developing nanosheets of 2D COFs, namely covalent organic nanosheets (2D CONs) in recent years[24] and being a class of layered materials, 2D COFs can be easily exfoliated into nanosheets compared to that of nonlayered 3D materials.[25] 2D covalent organic nanosheets (2D CONs) are now being considered as a member of 2D nanomaterials.[26] Like other 2D nanomaterials, their large surface area in 2D CONs allows greater absorption of drug molecules as well as superior control over release kinetics while their extreme thinness allows breakthroughs in biosensing and bioimaging. Many recent articles have reported about various applications of COFs.[27] In this article, we have discussed a general overview of 2D COFs in terms of commonly used chemical linkages and building blocks, their evolution toward chemically robust 2D COFs, general synthetic strategy to prepare bulk and nano 2D COFs and different aspects of their modular natures. Next, we have summarized the recent advances in biomedical aspects of this new class of porous 2D nanomaterials highlighting the principles and strategies involved. Finally, the future challenges toward achieving smart design or formulation of 2D COFs for advanced biomedical applications are discussed.

2. Types of 2D COF Based on Linkages and Their Relative Chemical Stability

A wide range of COFs with different linkages and molecular building blocks has been reported, which has been discussed in detail in many other reviews.[27a-d,28] Some of the widely used building blocks and linkages for 2D COFs are listed in **Figure 2** and **Table 1**. Typically, COFs are synthesized via reversible condensation of molecular building blocks.[4] The reversibility of the condensation reaction among the building blocks provides room for error correction by allowing rearrangement of the frameworks via cleavage & reformation of the newly formed bond. This scope for error correction during lattice formation imparts high crystallinity toward these 2D COFs, while the covalent characteristic imparts high thermal stability. In this section, we will discuss briefly about different linkages and molecular building blocks of 2D COFs.

Sukanya Bhunia is currently working as a postdoctoral research associate with Prof. Akhilesh Gaharwar at Texas A&M University (USA). She received her Ph.D. in Chemical Science from Indian Institute of Chemical Technology, Hyderabad (India) and Masters in Chemistry from the Indian Institute of Technology (IIT) Kharagpur (India). She is presently developing 2D covalent organic framework (COF)-based biomaterials for tissue engineering and drug delivery applications.
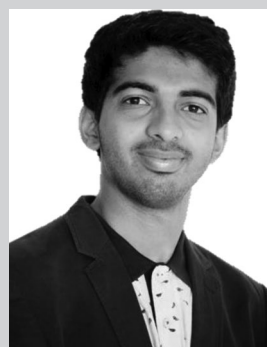
Kaivalya Deo is currently a doctoral student in the Department of Biomedical Engineering at Texas A&M University (USA). He received his bachelor's degree in Metallurgical and Materials Engineering from Visvesvaraya National Institute of Technology (VNIT), Nagpur (India). The goal of his research is to design nanoengineered biomaterials to direct cellular functions for a range of biomedical applications including regenerative medicine, drug delivery, and additive biomanufacturing. In addition, he aims to develop a physiologically relevant 3D printed tissue model to evaluate therapeutic interventions.

Akhilesh K. Gaharwar is an associate professor in the Department of Biomedical Engineering at Texas A&M University (USA). He received his PhD in Biomedical Engineering from Purdue University and completed his postdoctoral training from Massachusetts Institute of Technology (MIT) and Harvard University, USA. The goal of his lab is to understand the cell–nanomaterials interactions and to develop nanoengineered strategies for repair and regeneration of damaged tissue. In particular, his lab is leveraging principles from materials science, stem cell biology, additive biomanufacturing, and high-throughput genomics to design nanoengineered biomaterials, with wide-ranging applications in the field of regenerative medicine and drug delivery.
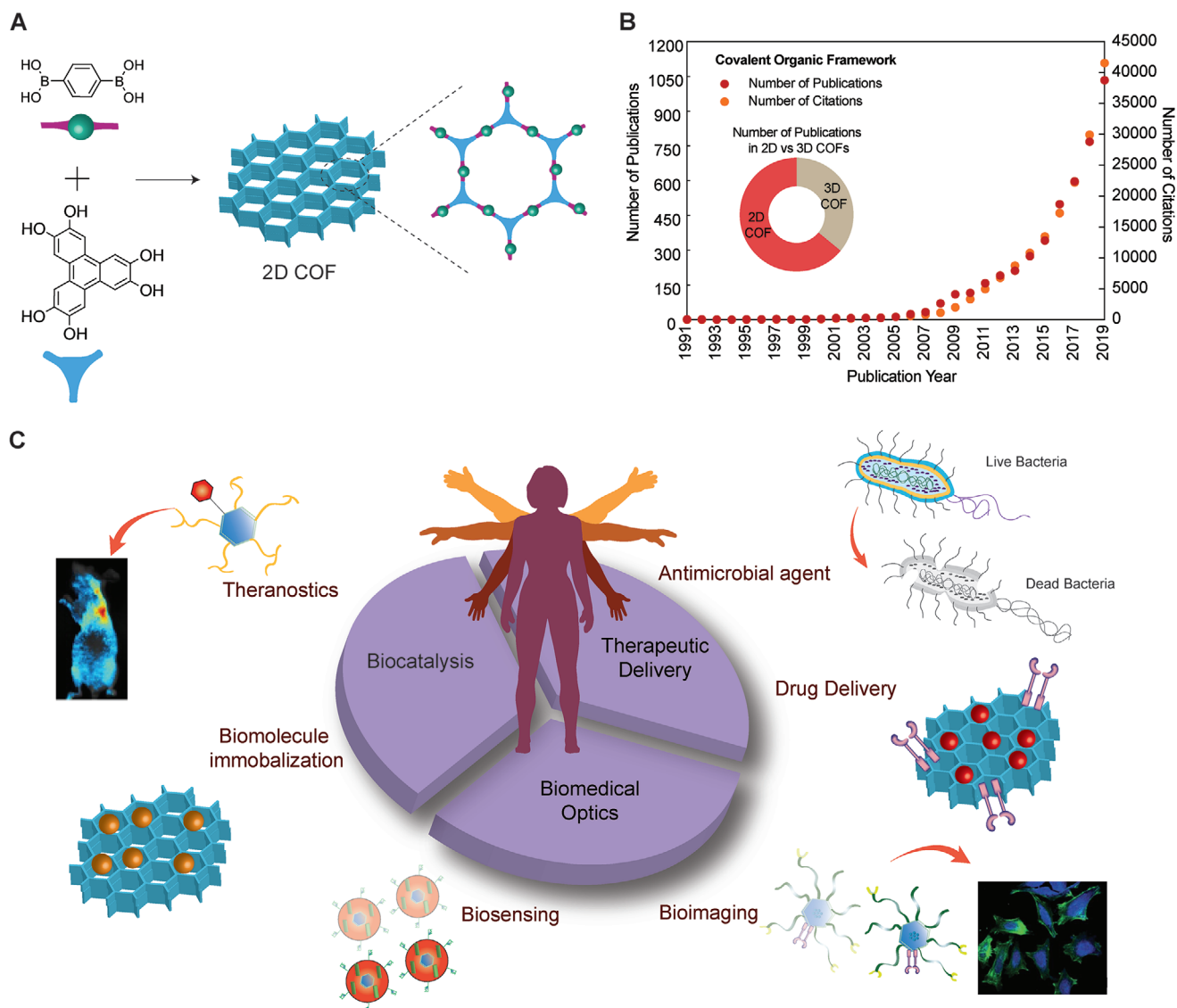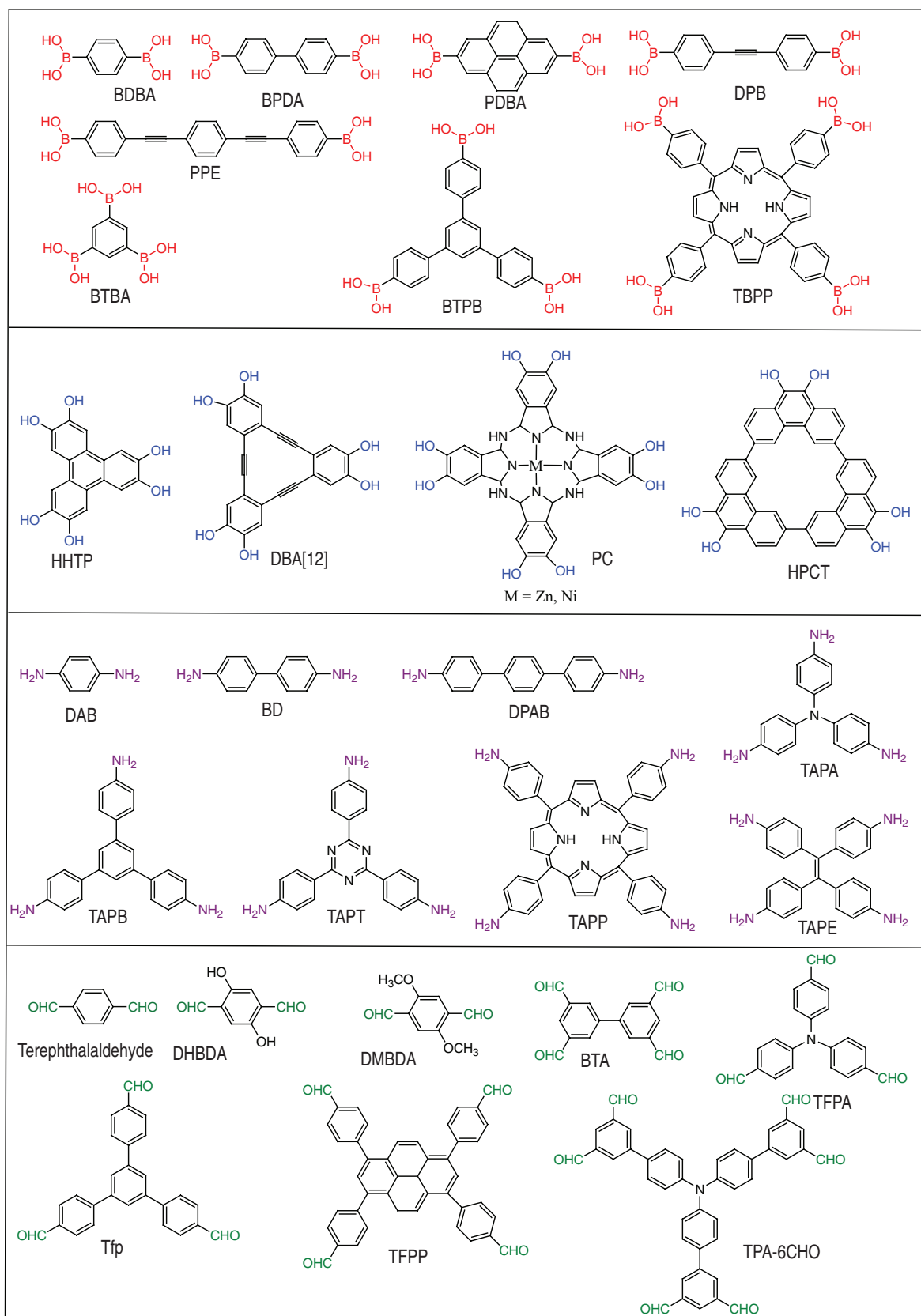
Figure 1. Biomedical applications of COFs. A) Schematic showing typical structure of a 2D COF. B) The number of publications in the field of COF and ratio of 2D COF and 3D COF according to ISI Web of Science (data obtained December 2019). C) The biomedical applications of COFs.

2.1. 2D COF Based on —B—O— Linkages

Boronic acid-based COFs are the first generation of 2D COF that was reported by Yaghi and co-workers.[4] Self-condensation of 1,4-benzene diboronic acid (BDBA) produces boroxine based networks of COF-1, whereas cocondensation of BDBA with 2,3,6,7,10,11-hexahydroxytriphenylene (HHTP) produces boronic ester-based hexagonal framework of COF-5. The reversibility of the condensation reactions comprising —B—O— linkages exhibited highly order structure and high thermal stability (500–600 °C) of these boronic acid-based 2D COFs. However, boronic acid-based 2D COFs are highly unstable toward trace of acid, alkali, alcohols, nucleophiles and even atmospheric moisture. Especially, the ultrasensitivity of boronate 2D COFs toward hydrolysis is a concern. For instance, Dichtel and co-workers have reported that boronate-based 2D COFs under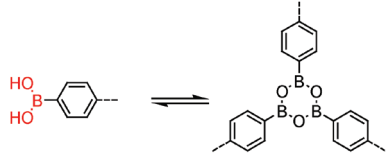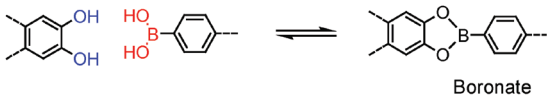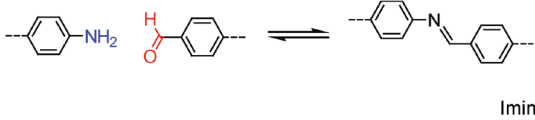go hydrolytic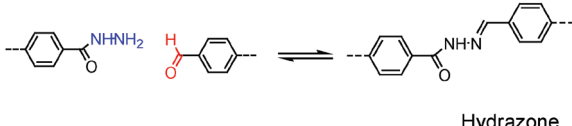 degradation by 50% within 11 s and by 90% within 1 min.[29] To enhance hydrolytic stability of boronic acid-based 2D COFs, Lanni and co-workers have reported a strategy of pore alkylation which enhances hydrolytic stability by 50% though its porosity and crystallinity was significantly compromised.[30] Another interesting strategy to improve the hydrolytic stability of boronic acid-based COF-1 is stabilizing the electron deficient B sites. Du et al. have reported that hydrolytic stability of COF-1 can be enhanced via amine functionalization of COF-1 using an aminosilane namely, (3-aminopropyl) triethoxysilane (APTES).[31] Here, the amine group of APTES stabilizes the electron deficient B sites via both Brønsted and Lewis interactions. In 2016, the same group has reported another strategy of stabilizing the electron deficient B sites through formation of spiroborate linkage leading to ionic 2D COFs containing sp³ hybridized boron anionic centers.[32] They have demonstrated that this ionic 2D COFs system with spiroborate linkage shows resistance to hydrolysis in water as well as
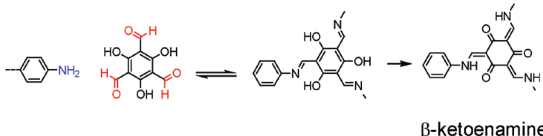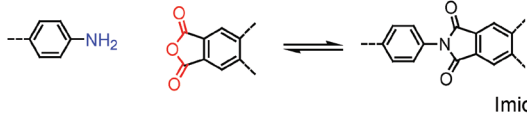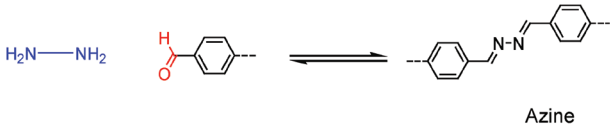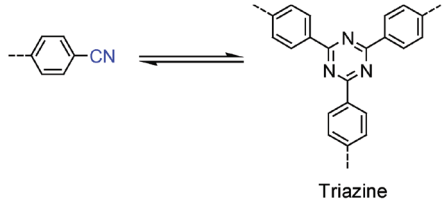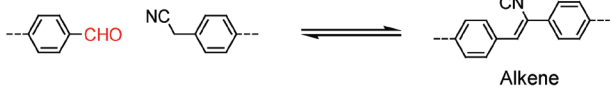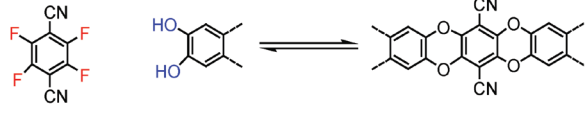
ADVANCED
SCIENCE NEWS
www.advancedsciencenews.com

ADVANCED
FUNCTIONAL
MATERIALS
www.afm-journal.de

Figure 2. Commonly used molecular building blocks (MBB) including boronic acid-based MBB (first row), diol based MBB (second row), amine-based MBB (third row) and aldehyde based MBB (fourth row) for the synthesis of 2D COF.

**ADVANCED
SCIENCE NEWS**
www.advancedsciencenews.com

**ADVANCED
FUNCTIONAL
MATERIALS**
www.afm-journal.de

Table 1. Types of linkages used for building 2D COFs.

Linkages		Characteristics			Refs.
		Crystallinity	Thermal stability	Chemical stability	
—B—O—	Boroxine	Excellent	500 °C	Highly sensitive to water, acid, base and nucleophile	[4]
	Boronate	Excellent	600 °C	Highly sensitive to water, acid, base and nucleophile	[4]
—C—N—	Imine	Good	500 °C	Better than boron-based COF	[33]
	Hydrazone	Good	280 °C	Better than imine-based COF	[35]
	β-ketoenamine	Good	350 °C	More than 7 days in boiling water, 9 M HCl and 9 M NaOH	[36]
	Imide	Good	530 °C	Better than boron-based COF	[41]
	Azine	Moderate	250 °C	1 day in water, 1 M HCl, 1 M NaOH and organic solvents	[43]
	Triazine	Poor	400 °C	High stability	[45]
—C—C—	Alkene	Moderate	350 °C	Stable in 12 M HCl, 55% aqueous KOH, 1 M nBuLi for 1 d	[48]
—C—O—	Ether	Moderate	No data	Most stable and robust COF reported so far	[50]

2002046 (5 of 27)

**ADVANCED
SCIENCE NEWS**
www.advancedsciencenews.com

**ADVANCED
FUNCTIONAL
MATERIALS**
www.afm-journal.de

in 1 M LiOH for two days, however, it decomposes in acidic and strong alkaline medium.

2.2. 2D COF Based on —C—N— Linkages

2.2.1. Imine-Based 2D COF

To overcome the limitation of hydrolytic instability of boron-based 2D COFs, a new class of imine-based 2D COFs is designed via condensation of molecular building blocks containing aldehyde and amine functionalities.[33] The higher stability of imine bond (—C—N—) compared to that of —B—O— in combination with extended π-conjugation throughout the 2D framework impart much better chemical stability of imine-based COFs and thereby provide a scope of wide range of applications. However, crystallinity of these imine-based 2D COFs is compromised compared with that of boronic acid-based 2D COFs due to limited reversibility of aldimine condensation reaction when compared to boronic acid condensation.

In 2011, Yaghi and co-workers have first reported an imine-based 2D COF formed via aldimine condensation of terephthaldehyde and tetra (p-amino-phenyl) porphyrin (TAPP).[33] The extended planar π-conjugation among the porphyrin moieties of this layered-sheet like 2D COF enables excellent charge carrier mobility. In the same year, Wang and co-workers have reported another imine-based 2D COF synthesized via reversible condensation of 1,4-phenylenediamine (PDA) and 1,3,5-triformylbenzene (TFB) arranged in a layered-sheet like structure forming hexagonal 1D-pore channels similar to that of COF-5 and showed their application in catalysis.[34]

2.2.2. Hydrazone-Based 2D COF

Hydrazone linked 2D COFs, another class of —C—N— based COFs, have been also synthesized via aldehyde–hydrazide condensation, which shows further enhanced hydrolytic & oxidative stability through extended H-bonding from hydrazide moiety in the pore spaces. In 2011, Yaghi and co-workers have first reported the synthesis of hydrazone linked 2D COFs, namely COF-42 & COF-43, via acid-catalyzed reversible condensation of 2,5-diethoxyterephthalohydrazide with 1,3,5-triformylbenzene and 1,3,5-tris(4-formylphenyl) benzene, respectively.[35] Afterward, a library of COFs with different pore geometry as well as pore diameter have been designed and synthesized leading to —C—N— based 2D COFs as most studied COFs so far.

2.2.3. β-Ketoenamine Based 2D COF

To further enhance the chemical stability of COF in water, Banerjee and co-workers first reported the synthesis of β-ketoenamine based COFs, another class of —C—N— based 2D COFs, in 2012.[36] Here, incorporation of a hydroxyl group to the β position of aldehyde functionality allows irreversible enol-keto tautomerism post COF formation, which imparts additional chemical stability to the 2D COF, while the reversibility of aldimine condensation maintains crystallinity of these

COF. Such 2D COFs are reported to be stable in 9N HCl up to 7 d. Furthermore, in certain class of β-ketoenamine based 2D COFs, such as β-ketoenamine based 2D COFs with porphyrin core[37,38] the β-hydroxyl groups form intramolecular H-bonding with adjacent Schiff base [—C—N—] centers. This approach minimizes interlayer repulsion of the 2D COF sheets via engaging lone pair of electrons of N-atom in intralayer H-bonding and eventually enhances the chemical stability of the 2D COFs. Thus, the enhanced stability in β-ketoenamine based 2D COFs has made it a popular class of 2D COFs developed so far and are widely being explored in diverse field.[39]

Incorporation of β-methoxy groups to the pore wall of imine-based 2D COFs may improve its chemical stability. In 2015, Jiang and co-workers have reported an imine based 2D COFs containing β-methoxy groups (TPB-DMTP-COF) where the resonance effect of methoxy group reduces the polarity of the imine bond.[40] This reduces interlayer repulsion observed in porous 2D COFs, which eventually enhances the stability of the TPB-DMTP-COF. TPB-DMTP-COF is demonstrated to show exceptional stability not only in boiling water and many organic solvents but also in strong acidic (12 M HCl) and strong basic (14 M NaOH) conditions. After 1 week of incubation of TPB-DMTP-COF in boiling water, 12 M HCl & 14 M NaOH, the residual weight percentages of TPB-DMTP-COF have been found to be 72, 85, and 92 wt%, respectively.

2.2.4. Imide and Amide Based 2D COF

The higher chemical stability of imide and amide bonds than that of imine bond triggers development of polyimide and amide based 2D COF. However, reversibility of the condensation reaction, which is a key criterion to form COFs become an issue leading to very few reports on 2D COFs with amide or imide linkage. Toward developing amide based 2D COFs, Yaghi and co-workers first synthesized imine based 2D COFs, which are then oxidized to the corresponding amide based 2D COFs.[41] The amide based 2D COFs are far more stable especially in acidic conditions (12 M HCl for 1 d) compared to their imine counterparts. Notably, this is the first report of post-COF synthetic chemical conversion. Similarly, a series of polyimide-based 2D COF has also been by Fang et al. with very large pore volume which shows temperature-dependent luminescence when doped with dye.[42]

2.2.5. Azine and Triazine Based 2D COF

Azine and triazine based 2D COFs are another class of 2D COF containing —C—N— linkages. The presence of conjugated linkage —C—N—N—C— in such azine and triazine based frameworks imparts additional chemical stability to 2D COFs. Azine based 2D COFs are formed via condensation of hydrazine and molecular building blocks containing aldehyde functionality. In 2013, Jiang and co-workers have first reported azine based 2D COF where condensation of 1,3,5,8-tetrakis(4-formyl phenyl) pyrene and hydrazine produces Py-azine COF containing rhombic pores of ≈2 nm diameter.[43] They have demonstrated that Py-azine COF is stable in weak acid (1 M HCl) and weak alkali (1 M NaOH) with no weight loss upon incubation.

Notably, the pyrene columnar ordering of Py-azine COF imparts high luminescent property in the frameworks. Later, the same group has reported a squaraine-linked 2D COFs, CuP-SQ COF, formed via condensation of squaric acid (SA) and copper(II) 5,10,15,20-tetrakis(4-aminophenyl)porphyrin (TAP-CuP) as a building block. CuP-SQ COF is demonstrated to be stable in water as well as in 1 M HCl for 1 d.[44]

Triazine based 2D COFs, also well known as covalent triazine-based frameworks (CTFs), are formed via cyclotrimerization of aromatic nitrile. In 2008, Thomas et al. have first described the synthesis of triazine based 2D COFs, CTF-1, via trimerization of 1,4-dicyanobenzene in a molten $ZnCl_2$ at 400 °C.[45] Later in 2010, the same group has reported CFT-2, the second member of triazine based 2D COFs formed via ionothermal condensation of 2,6-naphthalenedinitrile.[46] CTFs are reported to show excellent thermal, chemical and mechanical stabilities as of thermoset polymer material.[45] However, poor crystallinity and pore size distribution, as well as scalability due to harsh formation condition, are the major setbacks of CFTs although researches are going on to address scalability using a milder approach of synthesizing CFTs.[47]

2.3. COF Based on −C−C− Linkage and −C−O− Linkage

Recently, toward developing a chemically robust and graphene-like 2D material with tailorable magnetic and electronic properties Jin et al. have reported a fully π-conjugated C=C linkages based 2D COF.[48] The strong electron-withdrawing effect of nitriles attached to the C=C bond imparts reversibility to the C=C linkage, which may affect its chemical stability. This 2D COF and its chemically oxidized form have been reported as an excellent material for semiconductor applications. Later in 2019, Yaghi et al. have synthesized COF-701, another member of this 2D COF family via Brønsted acid-catalyzed aldol condensation between aryl aldehydes and the activated 2,4,6-trimethyl-1,3,5-triazine.[49] They have demonstrated that COF-701 is highly stable in acids (12 M HCl), bases (55% aqueous KOH & 35% methanolic KOH), and organolithium reagents including 1 M nBuLi in THF and 0.8 M MeLi in ethereal THF for 1 d. Only a minute loss of crystallinity is observed with COF-701 when exposed to more drastic conditions like n-BuLi/TMEDA taken in THF–hexane. Very recently, Guan et al. have reported a poly aryl ether-based 2D COFs (PAE-COFS), JUC-505 and JUC-506, as a new class of 2D COFs containing −C−O− linkage.[50] The excellent chemical stability of the ether linkage imparts excellent chemical stability to these 2D COFs. They have demonstrated that these PAE-COFs remain stable in even under extreme chemical environments including boiling water, strong acids (12 M HCl, 18 M H_2SO_4 and 40% HF), strong bases (14 M NaOH and 5 M sodium methoxide), and oxidizing (0.1 M chromic acid solution) as well as reducing (2.4 M $LiAlH_4$) conditions. As per the report these polyarylether based 2D COFs are not only the most stable 2D COFs developed so far but also more stable than all existing crystalline porous materials including aluminosilicate zeolites and metal-organic frameworks (MOFs).

Besides the linkages mentioned above, there are few other linkages such as borazine-linked[51] (−B−N− linkage) and other combinations of linkages including −C−N− & −B−O−,[52] −C−C−, & −B−O−[53] that are explored for the synthesis of 2D COFs. However, chemical stabilities of such 2D COFs are not studied in detail.

3. Synthetic Approaches of Bulk and Nanodimensional 2D COFs

In this section, we will first discuss the general synthetic approaches for bulk 2D COFs and next, we will discuss about the procedures to obtained nanoscale 2D COFs of biomedical relevance.

"Bottom-Up" Strategy to Synthesize Bulk 2D COF: A range of synthesis approaches is developed to obtain 2D COFs (**Figure 3**). Solvothermal synthesis is the most popular synthetic method to obtain 2D COFs. In this method, precursor monomers along with solvents and catalysts or modulators (if required) are allowed to react at high temperature (generally 75 °C–120 °C) in a closed container. The choice of solvents is very crucial for solvothermal synthesis and mostly mixed solvents are used, which can partially dissolve the precursor monomers.[28a] Enhanced solubility of the precursor monomers facilitates nucleation of the crystalline network, while the closed reaction system allows sustained supply of H_2O for maintaining reversibility of the condensation reaction to a crystalline elongation. Heating of the reaction mixture above the boiling point of the solvents increases solubility of the precursors and thereby improve reaction kinetics. Major domain of crystallinity (till 0.5 μm) can be achieved in this synthetic method. Solvothermal method of COF synthesis provides better control of crystallinity, porosity, and morphologies. However, scale-up and slow reaction rates are real challenges for industrial applications. Furthermore, this method needs a great deal of organic solvents (e.g., only 2% of reactant in solvent), which may lead to environmental concern.[54]

In ionothermal synthesis, ionic liquids facilitate COF lattice formation by acting as solvent as well as template or structure-directing component.[45–47] Kuhn et al. have first reported ionothermal synthesis of traizine linkage based 2D COF, namely CTFs, via cyclotrimerization of aromatic nitrile building block in molten $ZnCl_2$ at 400 °C.[45] Here, $ZnCl_2$ not only acts as a solvent but also as a catalyst for the cyclotrimerization reaction. These CTFs are mostly amorphous and show high thermal stability, which affords their wide application in catalysis. However, the harsh reaction condition limits the crystallinity of those materials.

Another approach to synthesize COFs is microwave-assisted synthesis. Campbell et al. have first reported the microwave-assisted synthesis of COF-5.[55] This approach is similar to the solvothermal process, where precursor monomers are dissolved in mixed solvents, sealed in a closed reaction vessel under nitrogen atmosphere and heated at 100 °C by microwave irradiation for 20 min. This method can produce COFs similar to that produced in classical solvothermal methods, while significantly reduces the reaction time. Microwave-assisted synthesis has also been used to prepare other classes of 2D COFs including β-ketoenamine[56] triazine[47] and melamine[57] based COFs.
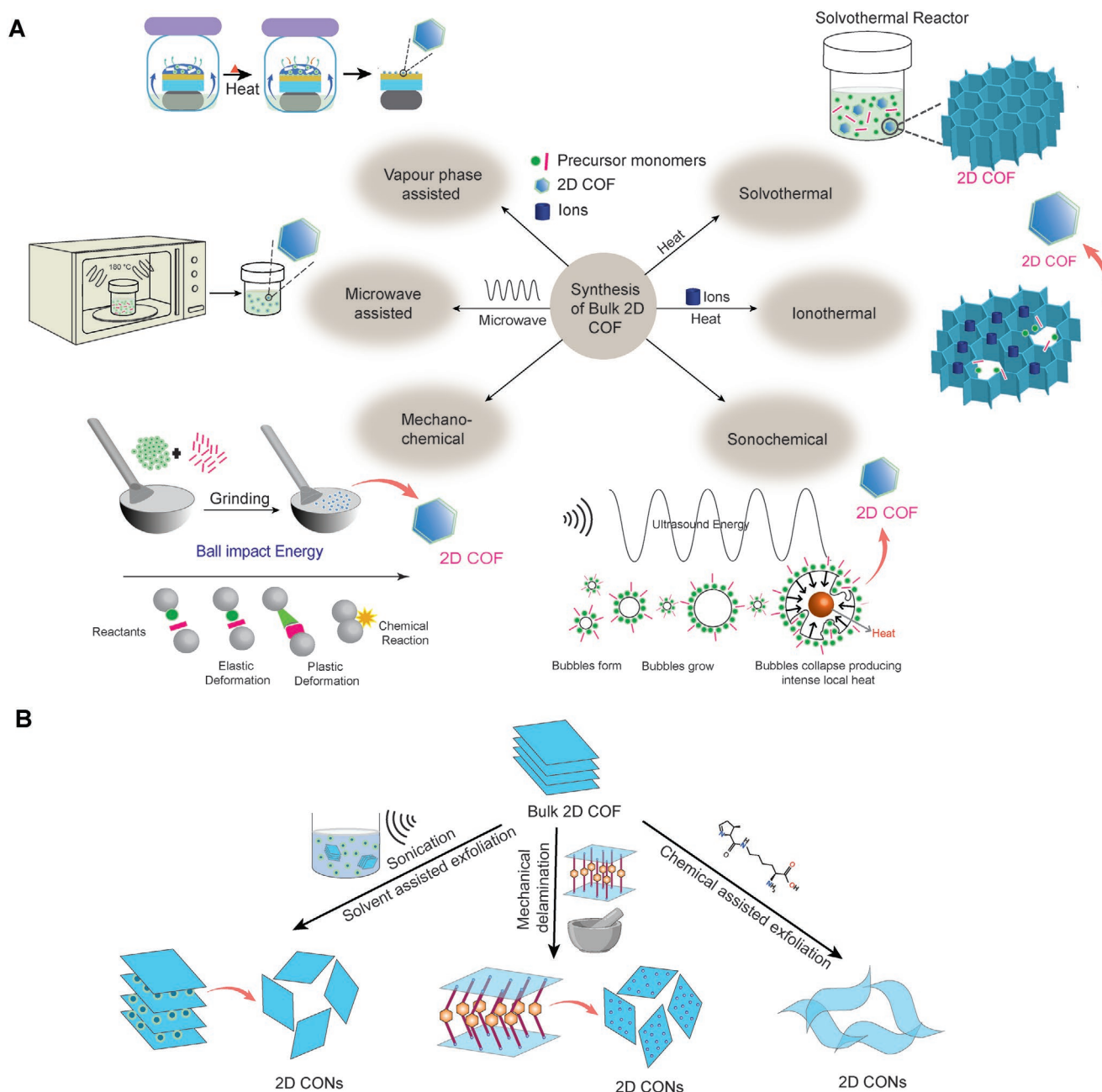
Figure 3. Synthetic approaches for bulk 2D COFs and covalent organic nanosheets (CONs). A) Bulk 2D COFs are synthesized from their precursor monomers in different methods, such as solvothermal, microwave, ionothermal, sonochemical, mechanochemical, and vapor-phase-assisted synthesis. B) Covalent organic nanosheets (CONs) are prepared from bulk 2D COFs (synthesized as above) via solvent-assisted exfoliation, mechanical delamination or chemical assisted exfoliation.

Simply mechanical grinding of precursor monomers with mortar and pestle can also produce same COF structures as obtained from solvothermal reactions. This method is known as mechanochemical synthesis and generally, it is used to prepare some β-ketoenamine based 2D COFs. Upon mechanical grinding, the precursor monomers undergo elastic and plastic deformation eventually leading to chemical reaction producing COF. In 2013, Banerjee and co-workers first reported the mechanochemical synthesis of β-ketoenamine-based 2D COFs by manually grinding two precursor monomers in a mortar and

pestle at room temperature.[58] Interestingly, progression of the reaction can be monitored visually by observing the intensity of color change leading to deep-red coloration, which confirms completion of the polycondensation reaction. Notably, the 2D COFs that are synthesized mechanochemically are obtained in a form of exfoliated thin sheets, which can also be obtained through the grinding of bulk 2D COF synthesized solvothermally. Although chemical stability of such COFs produced by this solvent-free greener approach is equivalent to that of solvothermally synthesized COFs, their crystallinity, as well as

BET surface area, are significantly compromised.[59] To enhance BET surface area and crystallinity of such COFs, a liquid-assisted grinding method has been developed. Addition of a catalytic amount of liquid to the mixture of precursors monomers enhanced the reaction rate. Imine and hydrazine based 2D COFs can be successfully synthesized using this method. The same research group has also reported an exceptionally rapid mechanochemical synthesis of ketoenamine based 2D COFs by grinding the diamine precursor together with *p*-toluenesulfonic acid (PTSA) (acting as molecular organizer) first followed by aldehyde precursor (1,3,5-triformylphloroglucinol) and water and heating the whole mixture to 170 °C only for 1 min. Interestingly, the dough formed out of properly mixed reagent ingredients can be molded into different shapes.[60] In addition to the synthesis of COFs mechanical stress can also facilitate aligning presynthesized unoriented 2D COFs powder into anisotropic packing.[61]

Similar to heat mediated synthesis 2D COF can also be synthesized by applying ultrasound, which is known as sonochemical synthesis. Ultrasound wave creates bubbles in the solution that undergo growth and implosive collapse in a process called acoustic cavitation, resulting in extreme elevation of local pressures and temperatures in the solution which further accelerates the condensation reaction. This approached has been used to synthesized boron-based COFs, COF-1, & COF-5, and is demonstrated that it can significantly reduce the reaction time to 2 h while maintaining the desired BET surface area with a scale-up capacity till 0.5 L batches.[62] This method can also be used in coating of COF-5 around carbon nanotubes and graphene.[63] Although this method is potential for boronic acid-based COFs, this has not been explored to the other types of linkage yet.

Vapor-assisted conversion of precursor monomer is another method of synthesizing 2D COF thin film on an interface. In this method, precursor monomers (for instance HHTP and (4,8-diethoxybenzo[1,2-b:4,5-b']dithiophene-2,6-diyl)diboronic acid)[64] are solubilized in low boiling solvents (such as mixture of ethanol and acetone), drop-casted on solid interface and then the whole system is kept inside a desiccator containing a reservoir of appropriate solvent systems (1:1 mixture of mesitylene and dioxane in this case) and incubated at room temperature for a definite period of time to prevail homogeneous films of 2D COF. Similar to solvothermal synthesis here also the choice of solvent systems in the reservoir determines crystallinity of the product. Vapor-assisted COF synthesis can also be successfully applied for precursor monomer mixed in their solid-state,[65] although COF obtained in this way may not remain in the thin film form.

Controlling Sizes and Morphology of 2D COFs: Controlling size and morphology while achieving processability remain a major challenge limiting many scopes of potential applications of COFs. Certain morphology or size of COFs is crucial for certain application toward harnessing their structural precision for the desired function. For example, morphologies like thin-film[27c] and few-layers structure are suitable for membrane and device-based application, respectively, whereas nanodimension is essential for drug delivery and other biomedical applications. However, COFs typically synthesized via heterogeneous polymerization of partially soluble monomers are often obtained as insoluble microcrystalline powders and therefore, these are

difficult to process into the desired size or shape. To address this issue, some strategies have been developed to produce COF in nanodimension, e.g., nanoparticles and nanosheets. Recently, Dichtel and co-workers have reported a strategy of homogenous polymerization to obtain boronate based 2D COFs in their stable colloidal nanoparticle suspension.[66] Upon screening of various cosolvent, the authors have found that using acetonitrile as cosolvent (in the solvent mixture of 1,4-dioxane and mesitylene) can prevent the precipitation of the resulting COF, which further leads to formation of stable colloidal nanoparticle suspension (≈50–200 nm depending on the ratio of acetonitrile) of these boronate based 2D COFs. Furthermore, authors have demonstrated that solution casting of these colloidal nanoparticle forms a free-standing film with preserved porosity as well as crystallinity indicating their ease of processability. It is worth mentioning that using this homogenous polymerization technique the authors have developed a seeded growth methodology (controlling nucleation/elongation of polymer via varying monomer addition speed) to obtain single crystal of large crystalline domain (0.5–1.5 µm) of 2D COF for first time.[17] The same group has also extended the strategy of homogenous polymerization via using acetonitrile as cosolvent to synthesize imine based 2D COFs as colloidal nanoparticles (≈200 nm).[67] Similar strategy of solvent-screening to obtain control over size, morphology as well as processability of 2D COFs is also reported by Zamora and co-workers.[68] The authors have demonstrated that aldimine condensation of 1,3,5-tris(4-aminophenyl)benzene and 1,3,5-benzenetricarbaldehyde at room temperature using *m*-cresol or dimethyl sulfoxide (DMSO) as solvent produce an imine based 2D COF, which can be fabricated on different solid surfaces (e.g., SiO_2) and can also be printed (ink-jet) on PDMS-based microfluidic chip. However, these 2D COFs can be obtained as sub-microsphere (≈600 nm) using acetone as solvent.

Zhao et al. have reported another interesting methodology of homogenous polymerization by using partially N-BOC (*tert*-butyloxycarbonyl group) protected amine building blocks, which get deprotected to amine in situ and thereby control rate of polymerization facilitating crystalline growth of COF.[69] Authors have validated this approach by using cobalt-complex supported homogeneous polymerization (aldimine condensation) to build a 3D-woven nanocrystal of COF. Guan et al. have also used similar strategy of such homogenous polymerization using partially N-BOC protected amine to obtain 2D COFs in their nanodimension which they have postsynthetically tagged with BODIPY for 2D COF mediated photodynamic therapy[70] (discussed in detail under 5.1). Another approach of obtaining nanodimensional 2D COF is "templated method" reported by Tan et al.[71] In this work, an amine based 2D COF has been fabricated on core–shell microsphere containing Fe_3O_4 nanocluster as core and polyamine as shell. This nanodimensional COF based hybrid material is demonstrated to show good photothermal efficiency through additional photothermal effect of π-electronic conjugation of stacked layers of 2D COF.

"Top-Down" Methods to Prepare Covalent Organic Nanosheets: Other than the "bottom-up" synthesis strategy mentioned above demonstrating different routes of synthesizing 2D COFs by combining precursor monomers there are also "top-down" synthesis methods especially used to produce thin-film or

nanosheets (CONs) of 2D COF from its bulk form. Bulk 2D COFs are composed of atomically thin 2D sheets stacked in layers, which are held via π–π interactions and/or H-bonding interaction. "Top-down" methods rely on breaking the interlayer interaction either via external or internal force to produce film or nanosheets of 2D COF and includes strategies like solvent-assisted exfoliation, chemical exfoliation, mechanical delamination, and self-exfoliation.

In solvent-assisted exfoliation external mechanical force, e.g., sonication is applied to the bulk 2D COF dispersed in a solvent. In presence of mechanical force, the solvent molecules intercalate between two adjacent layers, weaken the inter-layer π–π interactions and accelerates exfoliation. Solvent plays a crucial role in determining the exfoliation efficiency. A favorable surface tension between newly formed nanosheets of COF (CONs) and the solvent stabilized the CONs, which further facilitates exfoliation. For instance, Berlanga et al. have first reported[72] solvent-assisted exfoliation method to obtain nanosheets of COF comprising 10–25 monolayers from a boronate based bulk 2D COF, namely, COF-8.[73] Later on, this method has been extended to prepare CONs from hydrazine,[74] imine-linked 2D COFs,[75] and polyimide-linked 2D COFs.[76] However, if the dispersion stability of nanosheets is poor in solvents chemical exfoliation can produce a better exfoliation. For example, N-hexyl maleimide is used to obtain CONs from bulk anthracene based imine-linked COF DaTp.[24d] The [4 + 2] cycloaddition reaction between susceptible anthracene moieties of DaTp COF and N-hexyl maleimide weaken interlayer π–π interactions of DaTp COFs facilitating its exfoliation into nanosheets. Another effective method of obtaining CONs from 2D COF is mechanical delamination, which is first employed by Banerjee and co-workers[24a,58] During solvent-free mechanochemical synthesis of β-ketoenamine based 2D COF TpPa-1 and TpPa-2 authors have found exfoliated layers of 2D COF. Authors have demonstrated that mechanical forces during grinding weaken the interlayer π–π interactions and facilitates overcoming the peel strength leading to exfoliation of the bulk 2D COF into nanosheets.[58] Later on, this method has also been employed to obtain nanosheets from an anthraquinone based 2D COF (DAAQ-TFP-COF).[77] In contrast to the other "Top-down" methods mentioned above, self-exfoliation methods rely on the internal force, which can be tuned by incorporating bulky group or ionic moieties in the building blocks. For example, introduction of two methyl groups in triptycene tricatechol moiety induces interlayer steric repulsion, which further enables exfoliation of the 2D COF in monolayer thin films.[78] Similarly, introduction of cationic guanidium moiety to the building blocks facilitates self-exfoliation of 2D COF namely, TpTG$_{Cl}$ into iCONs via interlayer ionic repulsion of the same charge.[24c]

Other than the aforementioned strategies to obtain 2D COF in their "nano" dimension, there are other morphologies[65,79] reported in the literature including hollow microsphere, tubes, sea-urchin etc. obtained via random screening of reaction conditions out of which hollow microsphere is explored for biomedical purpose. For instance, Kandambeth et al. have reported an imine based 2D COF namely, DhaTab that shows reaction-time dependent morphologies.[80] The nano-rod produced after 12 h of reaction reforms it into microsphere (0.5–4 µm) at day 3–4 via inside-out Ostwald ripening to minimize th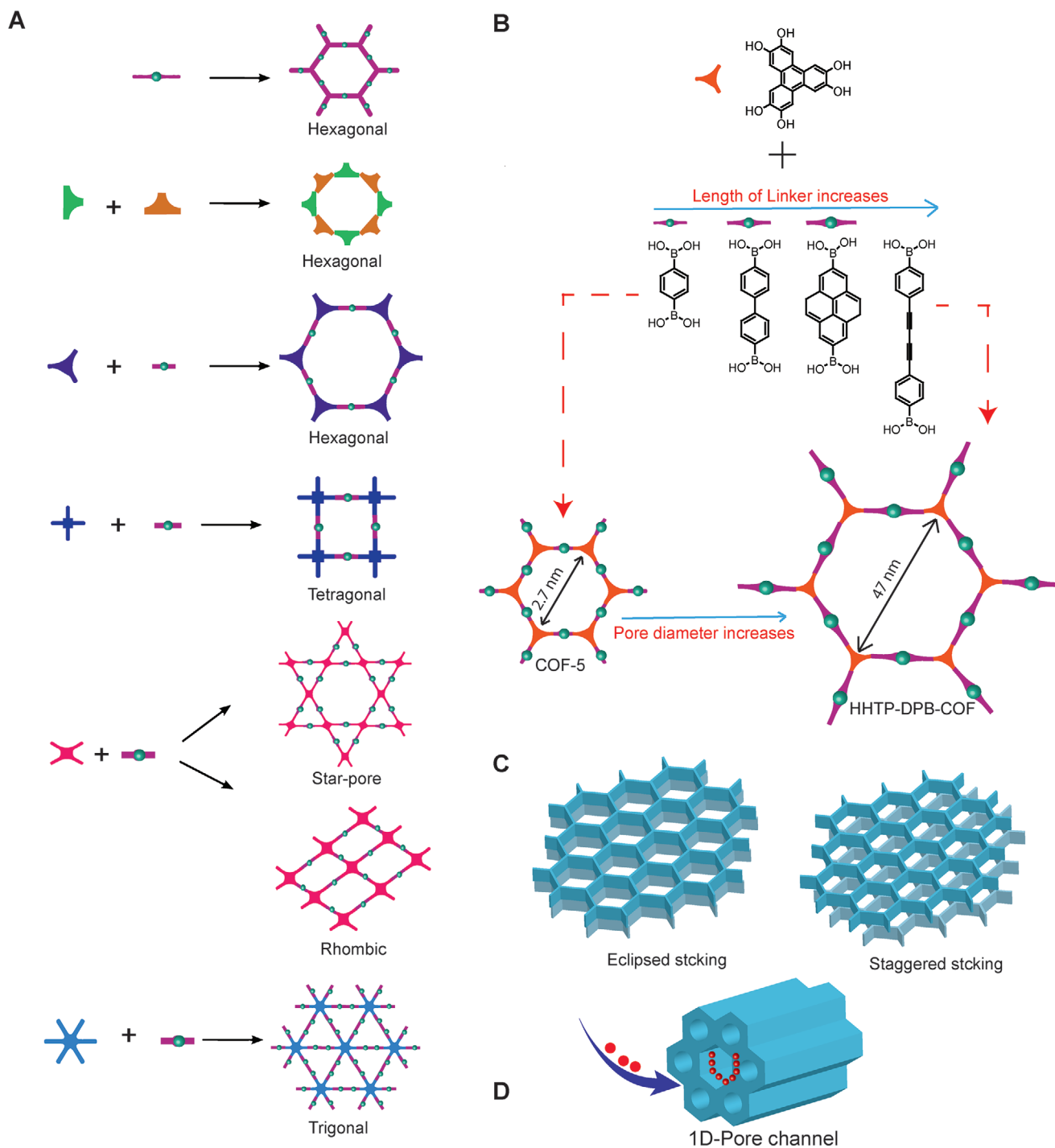e surface energy. These 2D COF-based microspheres are highly porous with a surface area of $\approx$1500 m^2 g^{-1} and can immobilize $\approx$15.5 µmol g^{-1} of trypsin. Yin et al. have also reported another COF based microsphere ($\approx$1 µm), which shows a high iodine uptake efficiency.[81] It is worth mentioning that "thin-film" morphology of 2D COF, although it is not relevant to biomedical purpose so far, is of immense importance for many applications including energy, semiconductor, membrane-devices, etc. and is the most studied one which is reviewed elsewhere in details.[27c]

Characterization Techniques: The 2D COFs can be chemically characterized using infrared radiation (IR), X-ray diffraction pattern (XRD), SAX/WAXS (for colloidal COFs) as well as X-ray photoelectron spectroscopy (XPS) whereas the latter is extensively used to differentiate CONs (nanosheets) from their bulk counterpart. Furthermore, atomic force microscopy (AFM) and transmission electron microscopy (TEM) are extensively used to confirm their morphology.

4. Tunability of COFs

The highly modular nature of COFs and MOFs has made these porous materials so unique. Properties of porous materials and their potential application often depend on size, shape, arrangement, and functionalities of their pore spaces. Prior to the development of MOF & COF, it has been a long challenge to develop porous materials where precise control of structure and function is possible simultaneously. With the development of MOF & COF, it has been possible to fine-tune the pore geometry, pore size, and functionality of pore wall, which can be leveraged to tailor their application.

In a COF lattice, the geometry of the framework is decided by the geometry and connectivity of molecular building blocks acting as linkers. For instance, self-condensation of trigonal planar linkers or its co-condensation with linear linkers constructs a network with hexagonal pores whereas tetragonal planar linkers co-condense with linear linkers to construct tetragonal pores (**Figure 4**A). Combination of planar linkers produces 2D sheets of COF, which further stack together in layers to form 2D COFs while the combination of linkers with connectivity in three dimensions (nonplanar linkers) produces 3D COFs. The commonly observed pore geometries in 2D COFs are listed in Figure 4A. Pore size of a 2D COF can also be tuned by varying length of linkers (as depicted in Figure 4B), which further determines the porosity of COF. Thus, the modular nature offers a broad range of micro-(<2 nm) and/or meso-(2–50 nm) porosity in those materials. For instance, COF-6 is the COF with the smallest pore of 8.6 Å and PC-COF is the COF with the largest pore size of 5.8 nm reported so far.[82] However, the porosity of 2D COF not only depends on pore size and geometry but also on pore arrangements in the framework, which is further controlled by layer stacking. If all the atoms of adjacent layers lie directly on top of each other it produces eclipsed (AA) stacking (Figure 4C-i) whereas if three-connected vertices of a pore lie on the geometric center of the pores from adjacent layers staggered (AB) stacking (Figure 4C-ii) is produced. Eclipsed stacking is the common pattern of stacking observed in 2D COF (only exception COF-1) which can well-arrange the pores to produce 1D pore-channel (Figure 4D). It is worth mentioning that as the pattern of layer stacking (either AA or AB conformations) depends on the interlayer

**ADVANCED
SCIENCE NEWS**
www.advancedsciencenews.com

**ADVANCED
FUNCTIONAL
MATERIALS**
www.afm-journal.de

Figure 4. Modular nature of 2D COFs. The porosity of 2D COFs can be modulated by tuning their pore geometry, pore size, the pattern of layer stacking and pore orientations, which are further dictated by choice of molecular building blocks. A) Commonly observed pore geometries in 2D COFs dictated by the topicity and geometry of molecular building blocks. Adapted with permission.[27b] Copyright 2018, Wiley-VCH. B) The pore size of 2D COFs can be tuned by tuning length of linkers. C) Layer stacking between two adjacent layers (either eclipse or staggered) and D) pore arrangements also determine the porosity of 2D COFs.

interactions within these 2D-COF materials, it can also be controlled, at an atomic level through the chemical design of the building blocks used in their synthesis.

The inner pore space of 2D COF can also be engineered to tune their functions. For instance, as discussed under Section 2.1 "alkylated pores" of boronic acid-based 2D COF prepared from alkyl-substituted benzene di-boronic acid as precursor improve its hydrolytic stability up to 50% compared to that of "bare pore."[30] Pore space can also be engineered post synthetically. For instance, Jiang et al. have introduced an azide group in the inner pore spaces of a boronic acid-based framework by adding azide- substituted benzene di-boronic acid to
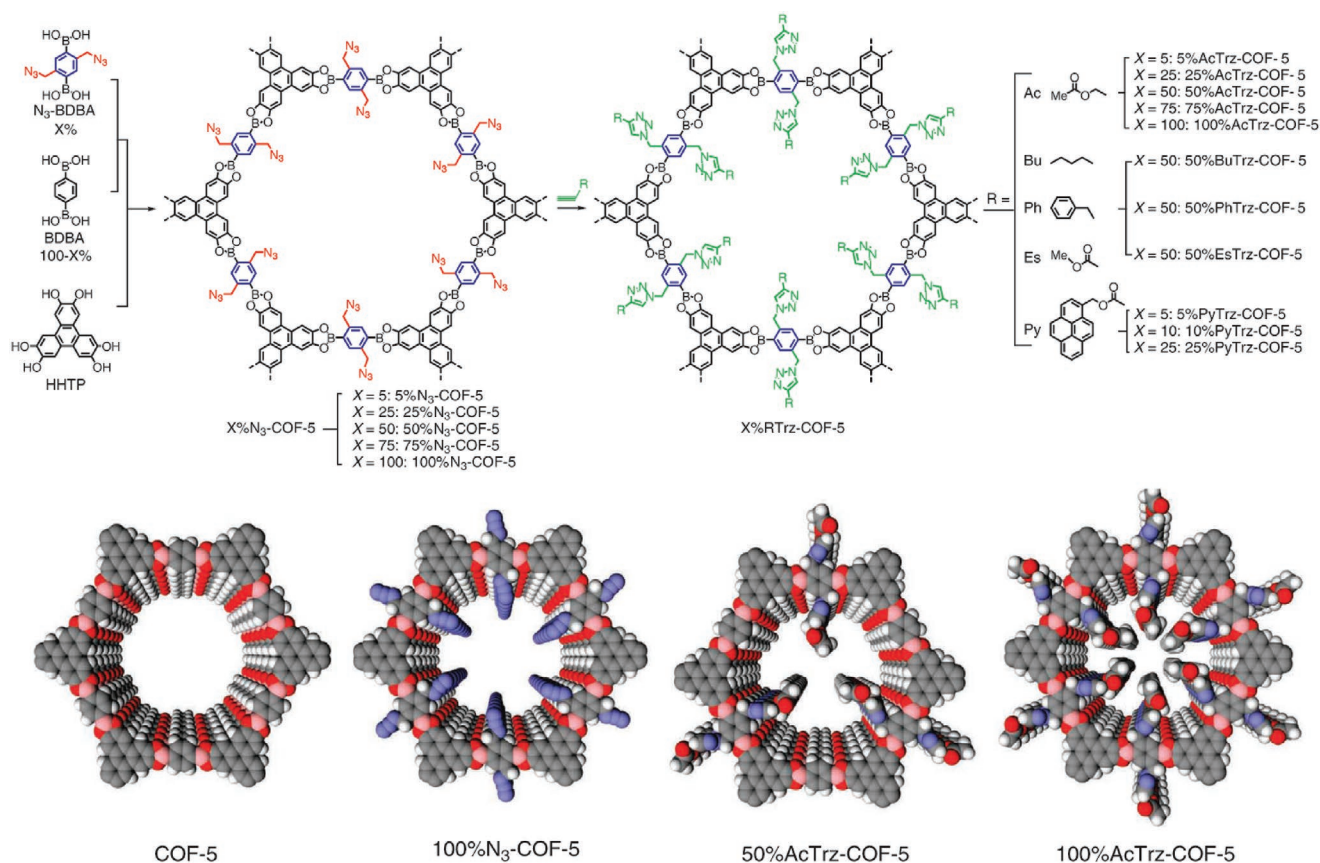
Figure 5. Inner pore space engineering of 2D COF to achieve different functionality. An azide group is introduced in the inner pore spaces of a boronic acid-based framework by adding azide substituted benzene diboronic acid to the reaction mixture of BDBA and HHTP in different ratios. The azide moieties can be further functionalized through click chemistry postsynthetically to incorporate different functionalities enabling the development of function-led 2D COFs. Adapted with permission.[83] Copyright 2011, Springer Nature.

the reaction mixture of BDBA and HHTP (**Figure 5**) in different ratios.[83] Postlattice formation the azide moieties can be further functionalized through click chemistry to incorporate different functionalities whose quantity can be again modulated by varying the percentage of the incorporated azide groups. This strategy of pore space engineering via click chemistry is demonstrated to fine-tune 2D COFs to achieve different energy related applications or catalysis. For instance, the same group has reported a porphyrin-based 2D COFs[84] and another phthalocyanine-based 2D COFs[85] which can be tailored postsynthetically for energy-related application via anchoring organic radicals[86] and electron-accepting fullerene (C_{60}) moieties, respectively, into the ordered 1D nanochannels of such 2D COFs. Similar strategy of inner pore space engineering has also been reported to tailor the functions of 2D COFs for heterogenous chiral catalysis[40,87] via anchoring chiral moiety and for mercury removal[88] via anchoring thiol functionality in the inner pore wall.

Not only the pore spaces, the skeleton, as well as surface of 2D COFs can also be tailored to fine-tune their functions. For instance, photoresponsiveness in 2D COFs can be introduced by incorporating "azo"-functionality[89] or anthracene unit[90] in the building block. Under UV light, the "azo" units of COFs undergo trans to cis isomerization resulting in opening of the framework whereas the anthracene units undergo interlayer [4 + 4] cycloaddition leading to structural transformation. In both cases, the initial

structures of 2D COFs can be regenerated by heating. Thus, the photoinducible switch for structural transformation and the thermoreversible regeneration of such "azo" or anthracene-based 2D COFs impart photoresponsiveness in those materials.

Photoelectric property in 2D COFs can also be introduced by modulating their skeleton using π-electron rich aromatic building blocks like pyrene, porphyrin, phthalocyanines, etc. The extended π conjugation throughout the planar framework sheet as well as the columnar ordering of the π-electron in the crystalline framework stacked in layers, make 2D COFs excellent photoeletric materials and thereby, make them suitable for chemosensing or phototherapy related application. Jiang and co-workers have first reported two pyrene-based 2D COFs with boronate linkage simply by replacing the BDBA blocks of COF-1 and COF-5 with pyrene 2,7-diboronic acid and demonstrated that these pyrene-based 2D COFs can exhibit luminescent and semiconducting property.[79a,b] Later, the same group has reported another pyrene-based luminescent 2D COFs with azine linkage,[43] which can act as fluorescence-based chemosensor for detecting explosive like 2,4,6-trinitrophenol via hydrogen bonding interaction with the azine unit. Similarly, the unique photoelectrical property and rich metal coordination chemistry of porphyrin and phthalocyanines moieties are explored as functional building block in designing 2D COFs with photoelectric property.[33,91]

The photoelectric potential of such 2D COFs can further be modulated by increasing the charge delocalization through donor-acceptor approaches[92] or by incorporating transition metal like Co, Ni, Cu, Zn, etc. into COFs at their coordination sites.[91,93] Incorporation of metal in COFs via coordination chemistry is one of the important strategies of modifying COFs, which not only modulates photoelectric property of 2D COFs but also holds great promise for application like gas storage[94] and catalysis.[34,95] Alkali metal such as Li, Na, K are generally incorporated in COFs to enhance gas storage capacity of COFs whereas transition metal like Co,[96] Zn,[95b] Mo,[97] Pd,[34] Ru[95a] or VO[98] and Co(II) ions,[99] are incorporated in 2D COFs for catalysis.

Apart from the inner pore space engineering and skeleton modification, 2D COFs can also be engineered at their surface presynthetically or postsynthetically. For instance, using truncated building blocks methodology, which is first reported by Bunck and Ditchel to internally modify a 3D-COF,[23b] outer surfaces of a 2D COFs can also be functionalized to fine tune their function. Using thiol or carboxylic acid functionalized phenyl-monoboronic acid as modulator, Bein and co-workers have developed an analogue of COF-5 containing thiol or carboxylic acid group at its exo-surface.[100] Also, to achieve tumor-targeted drug delivery, Banerjee et al. have reported post synthetic surface functionalization of a β-ketoenamine based 2D COF with folic acid which we will discuss in detail under Section 4.1. Thus, the development of covalent organic framework allows ample scope of tunability in a porous material to tailor these materials for a wide range of application.

5. Biomedical Applications of 2D COFs

For the past few decades, nanomaterials have enriched biomedical science in many ways including offering suitable drug delivery systems as well as several bioimaging and biosensing agents. A wide range of nanomaterials including organic materials (e.g., liposomes,[101] polymers,[102] dendrimer,[102d,103] etc.), inorganic materials (e.g., carbon,[104] nanosilicates,[105] mesoporous silica,[106] metal oxides,[107] etc.), as well as hybrid materials (polymer nanocomposite, hydrogel, etc.), have been designed and explored for therapeutic delivery, bioimaging, biosensing, and regenerative medicine. Some of these nanomaterials have already been approved by US FDA for clinical use (such as Doxil: liposomal doxorubicin, Abraxane: paclitaxel conjugated albumin NPs; Hafnium oxide (NBTXR3) has been approved in Europe for chemoradiotherapy of locally advanced soft tissue sarcoma); and many others are under clinical trials (such as iron oxide and gold for hyperthermia gene therapy and immunotherapy).[108] However, most of the biomaterials that show promises in preclinical studies failed in clinical trials mainly because of off-target effect, safety, and suboptimal efficacy. Although active targeting to the diseased tissue[109] and use of stimuli-responsive material[110] can reduce off-target effects, most of the nanomaterials produce acute toxicity[111] (especially inorganic materials) or adverse immunogenic response[112] because of their inherent toxicity and/or suboptimal drug content due to poor drug loading efficacy (e.g., liposomal carrier). These imitations lead to further need toward the search for new materials with better drug loading capacity as well as low toxicity. Particularly, the recent emerging

drift in nanoscience is focused on developing a new generation of smart materials, which are multifunctional, programmable, adaptive, and biocompatible. 2D COFs with their dual-advantages of porous polymeric nature as well as 2D geometry have multiple advantages as listed below for biomedical application:

1) The large surface, as well as high pore volume of 2D COF, enables high drug loading capacity: 2D COF poses much higher specific surface area than other class of porous material including silica and carbon-based porous material. For instance, specific surface area (BET) of COF-5 is 1590 m^2 g^{-1} (corresponding to a mesoporous volume of 0.998 cm^3 g^{-1}), which much higher than mesoporous silica-based porous material MCM-41 (680 m^2 g^{-1}) and even greater than that of macroporous ordered silica (1300 m^2 g^{-1}, the highest reported BET area) .[4] Additionally, being composed of polyaromatic compounds aromatic drugs can be easily loaded onto 2D COFs through π stacking interactions.

2) The reversibility of the covalent linkages enables a better scope of biodegradability: Unlike classical polymeric porous materials which are connected via irreversible covalent bonds, 2D COFs are connected through reversible dynamic linkages (such as $-B-O-$ and $-C-N-$), which allows better scope of biodegradability. Furthermore, these linkages often are broken in acid allowing a pH-responsive release of cargo.

3) Tunability: High tunability in terms of structure and function is the major advantage of using 2D COFs in nanomedicine. As mentioned above, the pores of 2D COFs can be fine-tuned in terms of size, shape via varying building blocks, which can be leveraged to further tailor the functions in terms of loading & release behavior towards different pharmaceuticals. Moreover, combination of linkages (e.g., $-C-N-$ & $-B-O-$ or $-C-C-$ & $-C-N-$) can also be used to construct new class of 2D COFs toward achieving optimum chemical stability, stimuli responsiveness as well as biodegradability. Finally, the surface of 2D COFs can also be engineered either via chemical conjugation or via formation of COF–polymer nanocomposite to achieve targetability or other properties crucial for biomedical application.

4) High π-electron density and large surface area of 2D COF enables excellent properties for phototherapy, biosensing, and bioimaging: Being composed of polycyclic aromatic unit-based building blocks (e.g., porphyrin or naphthalene), the extended π conjugation throughout the planar framework sheet and the columnar ordering of the π-electron of 2D COFs enable excellent photoelectric property in such materials. Furthermore, the large surface area of such nanoscale 2D COFs or 2D CONs allows better interaction with photoirradiation or biomolecules making them excellent candidates for phototherapy, biosensing and bioimaging. In addition to the characteristics mentioned above, 2D COFs outshines other pharmaceutically exploited ordered porous nanomaterials including mesoporous silica nanoparticle, titanium dioxide (nanoporous) and MOFs in terms of biomedical use as the former lack potential hazardous metal or silica part.

5.1. Drug Delivery

2D COF based drug delivery just has begun (**Table 2**). In 2016, Zhao and co-workers have examined the potential of

Table 2. Summary of 2D COF mediated drug delivery and phototherapy.

Year	COF	Linkage	Shape	Therapeutics	Key characteristics	Activity tested	Refs.
2016	PI-3-COF, PI-2-COF	Imine	Spherical (≈50 nm)	5-FU, captopril and ibuprofen	30% maximum loading efficiency with 5-FU	MCF-7	[113]
2016	TTI-COF	Imine	Elongated rod	Quercetin	Enhanced anticancer activity of drug loaded TTI-COF compare to free drug	MDA-MB-231	[114]
2016	COF$_{ABBA}$	Boroxine	Surface layer	Copper phthalocyanine	Photoresponsive COF	MDA-MB-231	[89b]
2017	TpASH-FA	βketoenamine	Nanosheets	5-FU	Targeted drug delivery	MDA-MB-231	[24b]
2018	TrzCOF	Imine	Nanorod (40–50 nm)		COF as anticancer agent	HCT-116	[115]
2018	PEG-CCM@APTES-COF-1	Boroxine	Nanodisk (120–150 nm)	Doxorubicin and curcumin	COF–polymer nanocomposite as theragnostic	HeLa cell & xenograft mouse model	[116]
2019	LZU-1-BODIPY-2I	Imine	Nanoparticle (≈100 nm)	BODIPY as photosensitizer Green LED light	Enhanced PDT efficiency via enhancing cellular uptake/tissue accumulation of PS when chemically conjugated to COF-nanocarrier	HeLa & MCF-7 cells, McF-7 xenografted mouse model	[70]
2019	ICG@COF-1@PDA	Boroxine	Nanosheet (diameter 170 nm, thickness 5.4 nm)	Indocyanine green as photosensitizer NIR laser	Enhanced PDT efficiency of PS by inhibiting its self-aggregation & quenching when loaded to COF-nanocarrier	Mouse subcutaneous tumor models of colorectal cancer and spontaneous lung metastas is of breast cancer	[117]
2019	COF-909	Imine	Nanoparticle (120–150 nm)	COF-909 as photosensitizer 630 nm Laser	COF itself as photosensitizer for PDT	CT-26 cells and mouse subcutaneous tumor model of colon carcinoma	[118]
2019	COF nanodots–PEG	Imine linkage Porphyrin as functional skeleton	Nanodots (≈4 nm)	COF nanodots–PEG 638 nm ± 10 nm laser	PEGylated COF nanodots as photosensitizer	HeLa cells & subcutaneous mouse tumor model of H22	[119]
2019	Py-BPy$^{+\bullet}$-COF/PEG	Imine linkage Pyrene as functional skeleton	Nanoparticle (164 nm)	Py-BPy$^{+\bullet}$-COF/PEG as photothermal agent 808 or 1064 nm laser	COF itself as photothermal agent that enables both of photoacoustic imaging and phototherapy	A549 tumor-xenografted in BALB/c nude mice	[120]
2019	COF@IR783@CAD	Boroxine	Nanoparticle (250 nm)	Cyanine for photothermal therapy with 808 nm laser Doxorubicin produg for chemotherapy	COF based carrier for combined photothermal and chemotherapy	4TI human breast tumor xenografted in nude mice	[120]
2019	VONc@COF-Por (3)	Imine	Nanoparticle (140 nm)	Porphyrinic photosensitizer and naphthalocyanine based photothermal agnet, 808 nm laser	COF as nanocarrier for photosensitizer and photothermal agent for combined PDT & PTT	MCF-7 cells and MCF-7 tumor xenografted in nude mice	[121]
2019	PEGylated COF-LZU-1–CuSe	Imine	Nanoparticle (150 nm)	CuSe as photothermal agent 650 & 808 nm laser	For combined PDT & PTT with COF acting as photosensitizer in presence of CuSe	In vivo tumor model of HeLa cells	[123]
2019	Hyaluronic acid functionalized COF-LZU-1-Ag$_2$Se	Imine	Nanoparticle (150 nm)	Ag$_2$Se as photothermal agent	For combined PDT & PTT with COF acting as photosensitizer in presence of Ag$_2$Se	In vivo tumor model of HeLa cells	[124]
2019	COF-366	Imine linkage Porphyrin as functional skeleton	Nanoparticle (100 nm)	635 laser	COF itself as combined PDT & PTT agent allowing photoacoustic imaging and combined phototherapy	4TI cells and its subcutaneous xenograft mouse tumor model	[124]

two imine-based 2D COFs, PI-3-COF & PI-2-COF, as a drug carrier in terms of their water dispersibility, biocompatibility, drug loading & release study as well as in vitro cytotoxicity.[113] Authors have demonstrated that these 2D COFs exist as spherical nanoparticle (size ≈50 nm) in water and show good biocompatibility. They have performed drug loading & release study using three different drugs including 5-fluorouracil (5-FU), captopril as well as ibuprofen. Drugs are loaded into COFs by incubating dried COF samples (solvent-free) with corresponding drugs in hexane solution under constant stirring for 6 h. Drug loaded COFs are characterized by PXRD, thermogravimetric analysis (TGA), and FTIR and drug loading efficiency is determined by TGA. Drug loading & release study indicate that there is a direct correlation between drug loading efficiency and pore size of 2D COF. High drug loading (up to ≈30%) efficiency is observed when PI-2-COF is loaded with 5-FU resulting in significant cytotoxicity in MCF7 cells. In the same year, Vyas et al. have reported another imine based 2D COF, namely TTI-COF (**Figure 6**A), synthesized from the mixture (1:1 molar ratio) of triazine triphenyl amine and triazine triphenyl aldehyde as precursor monomers.[114] The lone pair of electron on the imine nitrogen of TTI-COF are available for anchoring guest molecules reversibly, which leads to easy loading and conditional release of guest molecules in cells. They have explored the TTI-COF for delivery of quercetin (3,3′,4′,5,7-pentahydroxyflavone), an anticancer flavonoid into

MDA-MB-231 cells and have demonstrated that quercetin shows enhanced cell killing efficiency when loaded in TTI-COF compared to free quercetin over a period of 4 days of treatment. However, authors have not mentioned drug loading efficiency of TTI-COF (as quercetin is decomposed during TGA) although authors have performed FTIR, ^{15}N direct-excitation solid state NMR, nitrogen adsorption study (to determine BET surface area) of TTI-COF and quercetin loaded TTI-COF in support of drug loading. Furthermore, release study of quercetin in PBS (pH 7.4) cannot be performed successfully due to low solubility and oxidation prone nature of quercetin. Notably, this report emphasizes the importance of understanding the host–guest interactions in these new classes of porous crystalline framework and indicates their (2D COF's) promises as potential drug carriers beyond their conventional applications in gas storage and catalysis.

Stimuli responsiveness and targeted delivery of payloads are the indispensable characteristics of an ideal drug carrier. Toward developing stimuli-responsive COF, Lei et al. have demonstrated development of a boronate-based photoresponsive 2D COF containing photoresponsive azobenzene moiety in the backbone of diboronic acid.[89b] UV irradiation mediated isomerization of azobenzene group causes destruction on the surface of the framework leading to opening of the framework whereas annealing can recover the destabilized surface framework. This photoinduced switch of opening and closing of the
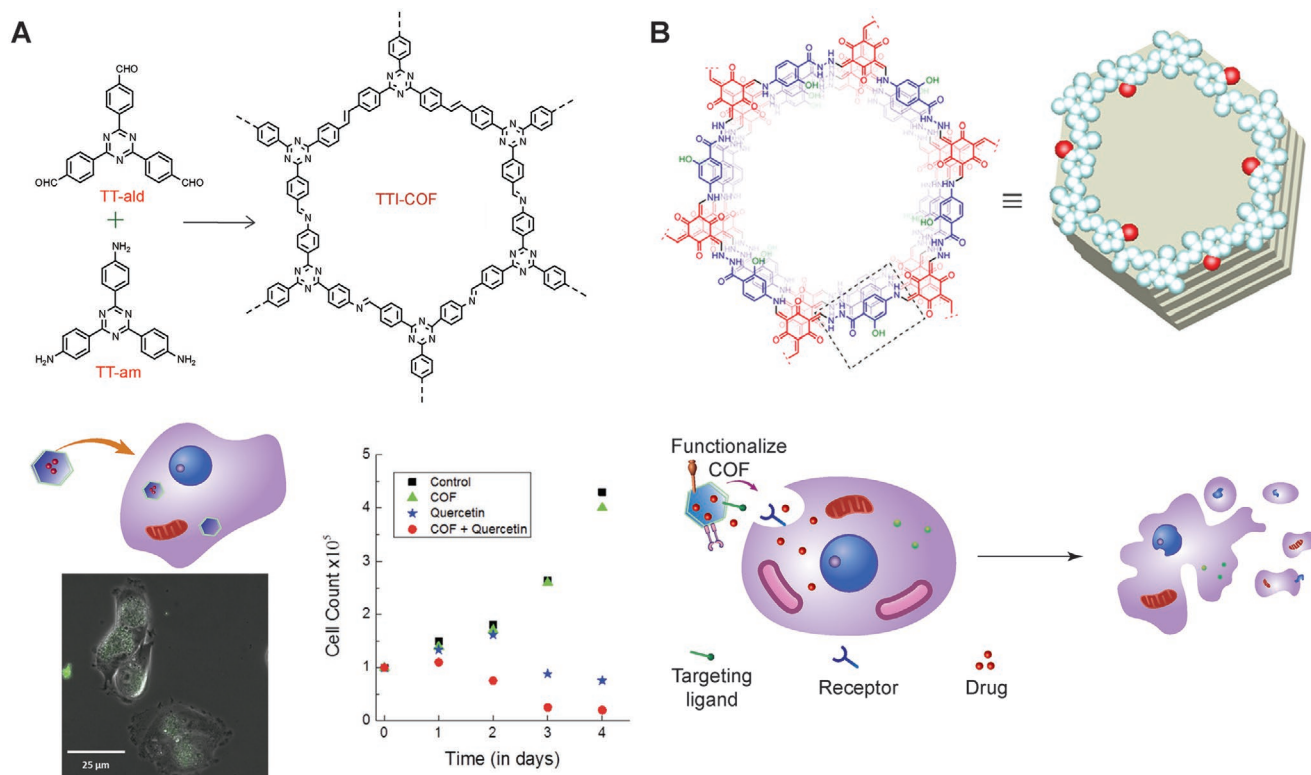
Figure 6. 2D COFs in drug delivery. A) An imine based 2D COF TTI-COF synthesized via aldimine condensation is explored for sustained delivery of quercetin in breast cancer cells resulting enhanced cell killing when cells are treated with quercetin loaded COF (COF + quercetin) compared to that of free quercetin or only COF. Adapted with permission.[114] Copyright 2016, Wiley-VCH. B) Postsynthetic modification of a β-ketoenamine based 2D COFs TpASH facilitates 2D-COF carrier based targeted delivery of 5-Fu in cancer cells via cancer selective internalization of 5-Fu through receptor mediated endocytosis resulting in enhanced cellular cytotoxicity. Adapted with permission.[24b] Copyright 2017, American Chemical Society.

ADVANCED
SCIENCE NEWS
www.advancedsciencenews.com

ADVANCED
FUNCTIONAL
MATERIALS
www.afm-journal.de

surface framework allows controlled loading and release of guest molecules, which is demonstrated by using copper phthalocyanine as a model guest.

To obtain targeting property in 2D COF, Banerjee et al. have reported postsynthetic modification strategy.[24b] A β-ketoenamine based 2D COFs, namely TpASH, (Figure 6B) is surface-functionalized with folic acid (a ligand for folate receptor) to produce folic acid functionalized 2D covalent organic nanosheets (2D CONs, thickness of 15 nm) of TpASH-FA and explored it for delivering anticancer 5-Fu selectively to breast cancer cells overexpressing folate receptor. Drug loading efficacy of TpASH-FA is found to be 12% as determined by UV–vis spectroscopy via estimating the unencapsulated drug in the supernatant solution. Sustained release of 5-Fu (release rate 74%) for 3 d is observed at pH 5, lysosomal pH of cancer cells. 5-FU loaded in TpASH-FA are selectively internalized by folate receptor-positive human triple-negative breast cancer cells MDA-MB-231 via folate receptor-mediated endocytosis and induces programmed cell death.[24b] It is worth mentioning that although drug loading efficacy of TpASH-FA is low compared to other 2D COFs discussed above this is the first report demonstrating postsynthetic modification of 2D COF facilitating its exfoliation to surface functionalized 2D CONs for targeted drug delivery.

Apart from a drug carrier, 2D COF itself can act as an anticancer agent. For instance, recently Bhaumik and co-workers have reported an imine based 2D COF, namely, TrzCOF, which itself shows anticancer activity in human colon cancer cells HCT-116.[115] TrzCOF has a nano rod-like morphology consisting of self-assembly of nanoflakes ranging ≈40–50 nm, which can be internalized in cancer cells through endocytosis. TrzCOF is screened for cytotoxicity against different cancer cells including mouse melanoma cells B16F10, human liver cancer cells HepG2, and human colon cancer cells HCT-116 in a varying concentration ranging from 1 to 80 μg mL^{-1}. TrzCOF shows the highest cell killing efficacy in HCT-116 cells with a 50% inhibitory potential (IC$_{50}$) of ≈8.31 μg mL^{-1} which is comparable with that of 5-FU (IC$_{50}$ ≈10.27 μg mL^{-1}) in the same cells. This cytotoxic effect of TrzCOF is independent of its precursor monomers and is mediated via generation of reactive oxygen species (ROS) in cells treated with TrzCOF, which further leads to DNA damage and initiates a cascade of signals resulting apoptotic death of cancer cells. However, it is important to know the effect of TrzCOF on healthy cells as well which authors have not addressed. It is worth mentioning that this study emphasizes the fact that 2D COF may have inherent cytotoxicity and here lies the importance of critically evaluating biocompatibility and systemic toxicity of 2D COF prior to their applications in pharmaceutics as a drug carrier.

2D COF has also been explored for drug delivery in complexation with the polymer. In 2018, Jia and co-workers have reported development of a COF–polymer nanocomposite as a water-dispersible drug carrier for in vivo tumor targeting of combination chemotherapeutics.[116] In this work, amine-functionalized —B—O— linkage based COF-1 (APTES@COF-1) is loaded first with doxorubicin and then complexed with pegylated curcumin (PEG-CCM), to form COF-polymer nanocomposite namely, PEG-CCM@APTES-COF-1. PEG-CCM@APTES-COF-1 self-

assemble to form micelles encapsulating Dox loaded COF-1 in their inner core coated by PEGylated curcumin at the outer layer (**Figure** 7A,B). PEG-CCM@APTES-COF-1 nanocomposites exhibit intense fluorescence (Figure 7C), which facilitates their tracking both in vitro cellular uptake study (Figure 7D) as well as in vivo tissue distribution upon intravenous injection in mice (Figure 7E). Eventually, in vivo antitumor efficacy of PEG-CCM@APTES-COF-1 nanocomposites encapsulating Dox is evaluated using a subcutaneous tumor model of HeLa cell xenografted in nude mice.[116]

5.2. Phototherapy

Nanoscale 2D COFs are also being explored in photodynamic therapy (PDT) and photothermal therapy (PTT). In PDT, photosensitizer (PS), a class of light-absorbing organic dye, are the therapeutic agents which in presence of light can convert molecular oxygen to cytotoxic singlet oxygen ($^1O_2$) which elicit cell death. In PTT, another class of light-absorbing compounds, known as photothermal agent, generates heat once irradiated with IR light which kills the cells. However, poor water solubility and instability, aggregation, occasional photobleaching, and low cell permeability of those organic dyes limit their therapeutic efficacy. The ordered pores of nanoscale 2D-COFs can be used as a platform for assisted dispersion of such organic dyes for enhancing their therapeutic efficacy. For instance, Dong and co-workers have developed a nanometric (≈110 nm) COF based photosensitizer namely, LZU-1-BODIPY-2I, by covalently grafting BODIPY photosensitizer at the bonding defect sites of nanodimensional 2D COF.[70] In presence of green LED light (1 W cm^{-2}), this nanoCOF based photosensitizer shows much enhanced therapeutic efficacy compared to corresponding naked photosensitizer in MCF-7 tumor xenografted in nude mice.

Another study have utilized the ordered pores of nanoscale 2D COF as platform for molecular dispersion of the photosensitizer, which can eventually increase the photodynamic efficacy by preventing quenching arising from π–π interaction mediated self-aggregation.[117] The authors have demonstrated that a 2D-COF based photosensitizer ICG@COF-1@PDA, prepared from indocyanine green (photosensitizer) loaded in APTES functionalized COF-1 and subsequently coated with polydopamine, exhibits enhanced photodynamic efficiency compared to naked indocyanine green in mouse tumor models of subcutaneously implanted colorectal cancer and spontaneous lung metastasis of breast cancer.

Some nanoscale 2D COFs can itself act as photosensitizer because of their excellent photoelectric properties arising from extended π conjugation and the columnar ordering of the π-electrons. For instance, Zhang et al. have developed a 2D COF based photosensitizer (namely, COF-909) synthesized from PDT inactive molecular building blocks designated as L-3N.[118] Upon crystalline framework formation, the band gap of the L-3N dramatically decreases from 2.79 to 1.96 eV in the COF-909 enabling its photo-excitation at 630 nm leading to ROS generation in presence of O_2 (**Figure** 8A-i). Importantly, the high porosity of COF-909 not only helps ROS generation via facile transfer of the photoelectron (generated from photo excitation) to O_2 in the pore environment but also helps easy diffusion of
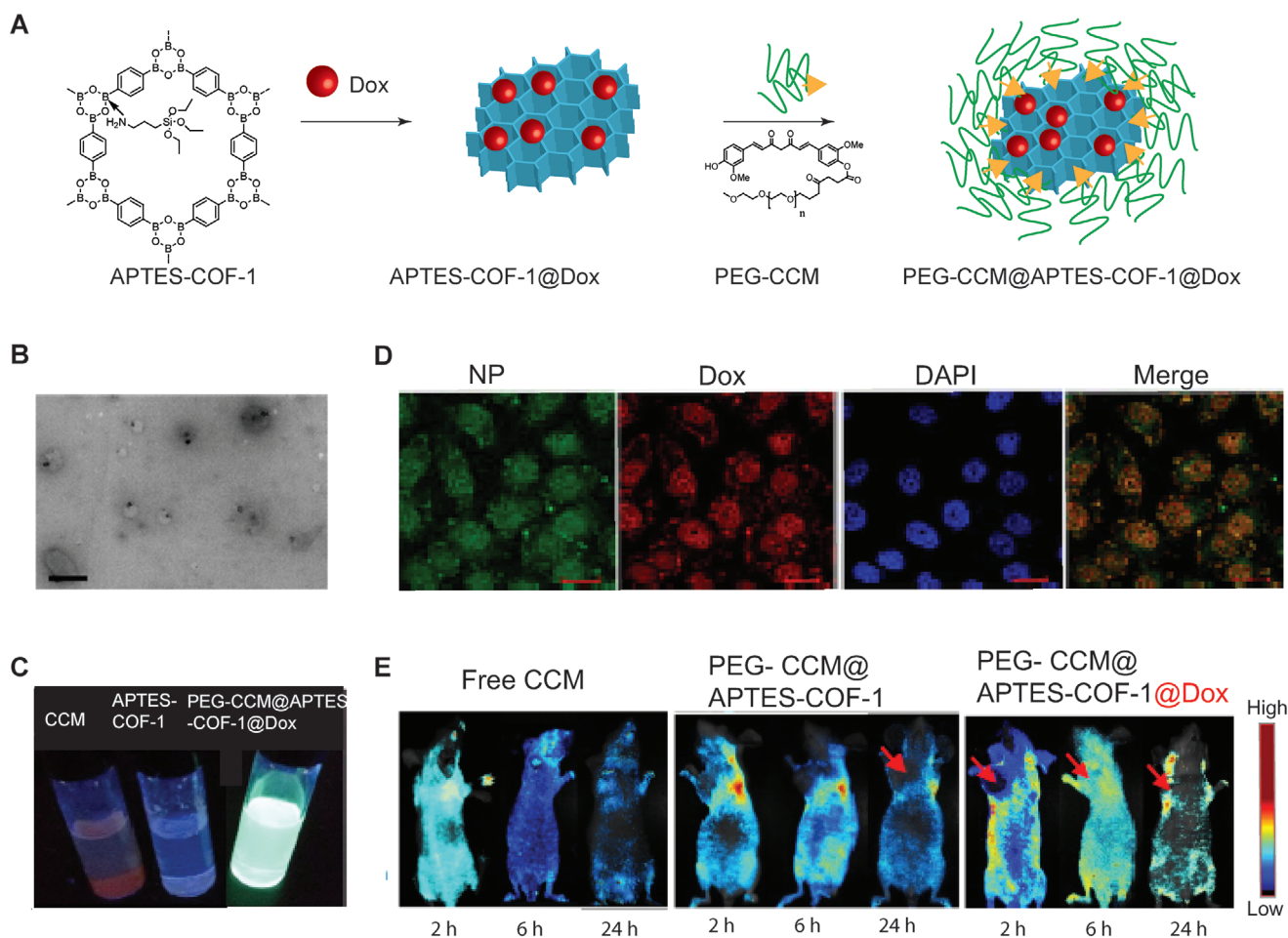
Figure 7. 2D COF–polymer nanocomposite based nanocarrier for in vivo tumor targeting of combination chemotherapeutics. A) APTES stabilized COF-1 is loaded with doxorubicin first and added with an amphiphile PEG-CCM, curcumin (CCM) chemically conjugated to polyethylene glycol (PEG) leading to self-assembly mediated formation of water-dispersible nanoparticle (NP) PEG-CCM@APTES-COF-1@Dox. B) Transmission electron micrographs of PEG-CCM@APTES-COF-1@Dox. C) Fluorescent nature of PEG-CCM@APTES-COF-1 enabling their trafficking in D) cellular uptake study under in vitro conditions as well as in E) pharmacokinetics study using a mouse model of tumor. B–E) Adapted under the terms of a Creative Commons Attribution CC-BY license.[116] Copyright 2018, The Authors, published by Springer Nature.

O₂ or ROS resulting impressive photodynamic behavior of this 2D COF. Authors have demonstrated high in vitro phototoxicity of COF-909 in CT-26 colon cancer cells as indicated by 80% of cells death when photoirradiated with 50 µg mL⁻¹ of COF-909 for 150 s. An impressive in vivo PDT efficiency of COF-909 is also reported as indicated by significant reduction of tumor burden from 9 to 1 mm and corresponding H&E staining of the tumor sections (Figure 8A-ii).

Aiming at high renal clearance and minimal in vivo toxicity of anticancer photodynamic therapy, Qu and co-worker have developed a PEGylated COF based nanodots (size ≈4 nm and thickness of ≈3 nm) via solvent mediated exfoliation of a porphyrin-based 2D COF.[119] Authors have demonstrated that the PEGylated COF based nanodots produces significant amount of ROS upon irradiation with 638 nm laser and examined their therapeutic efficacy using HeLa cells (in vitro) and H22 tumor-bearing mice (in vivo), respectively. Authors have demonstrated that the rationale behind using the ultrasmall COF based nanodots over 2D CONs to achieve high renal clearance profile

and to avoid in vivo toxicity. However, there is no information in this study regarding the probable in vivo toxicity or relative comparison of PDT efficiency between COF based nanodots and corresponding 2D CONs especially, when PDT efficiency depends on surface area of the photosensitizer as well as its EPR effect mediated accumulation in the target tissue, which generally works for the nanocarrier with diameter of 50–200 nm.

The highly modular nature of 2D COFs also allows their exploration in photothermal therapy both as individual photothermal agent (PA) or as a nanocarrier of PA. For example, Mi et al. have explored the potential of nanoscale 2D COF as photothermal agent for cancer theranostics.[120] Authors have developed a radical-cation containing 2D COF (Py-BPy⁺•-COF) via in situ reaction strategy which allows stabilization, delocalization, and uniaxial stacking of the radical via interlayer π-electronic couplings generating a columnar array of cationic π-radical (Figure 8B). The PEG functionalized water dispersible formulation of Py-BPy⁺•-COF (Py-BPy⁺•-COF/PEG) exhibits remarkable absorption property in the NIR
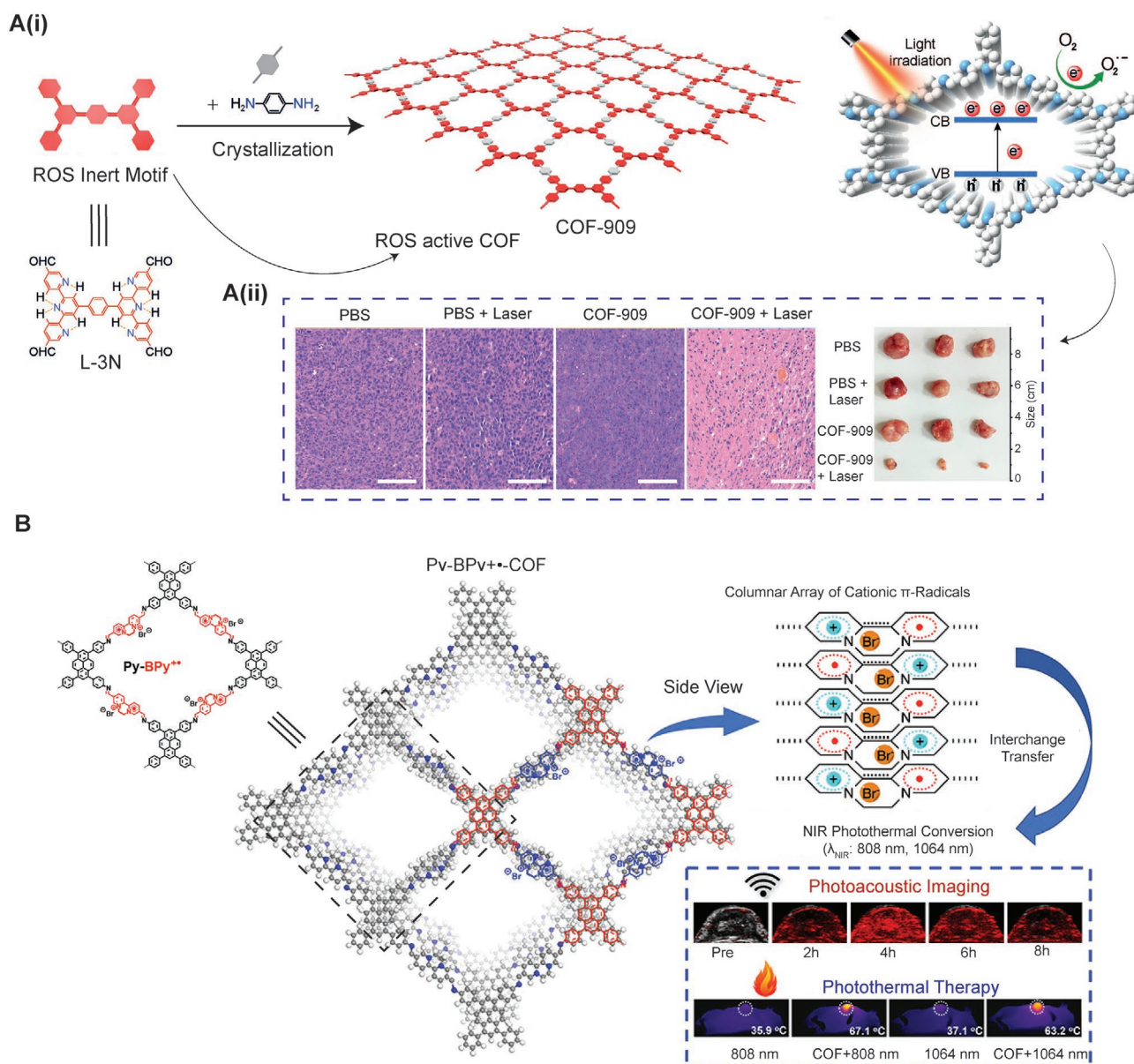
Figure 8. 2D COF in phototherapy. A-i) a photodynamic therapy (PDT) inactive molecular building block L-3N forms a PDT active covalent organic framework (COF-909) upon crystallization mediated molecular organization and generates reactive oxygen species (ROS) when irradiated with 630 nm light. A-ii) COF-909 exhibits significant in vivo PDT efficiency in mouse tumor model of colorectal cancer (CT-26) as indicated by the reduction of tumor burden from ≈9 to ≈1 cm and corresponding H&E staining in presence of Laser.[118] Images are adapted with permission Copyright 2019, Wiley-VCH. B) Framework formation in Py-BPy$^{+\bullet}$-COF enables stabilization, delocalization and uniaxial stacking of the cationic radical via interlayer π-electronic couplings resulting a columnar array of cationic π-radical. The PEG functionalized water dispersible formulation of Py-BPy$^{+\bullet}$-COF (Py-BPy$^{+\bullet}$-COF/PEG) exhibits a good photothermal therapy as well as photoacoustic imaging in mouse tumor model. Adapted with permission.[120] Copyright 2019, American Chemical Society.

range such as, high extinction coefficient of 16.6 L g^{-1} cm^{-1} and 15.9 L g^{-1} cm^{-1} at 808 and 1064 nm, respectively. This strong NIR light absorption in combination with observed low fluorescence quantum yield imparts good photothermal behavior in Py-BPy$^{+\bullet}$-COF/PEG resulting from nonradiative relaxation upon photoexcitation. Authors have demonstrated the in vitro photothermal efficacy of Py-BPy$^{+\bullet}$-COF/PEG by measuring its phototoxicity in human lung carcinoma

cells A549. Authors have also investigated the in vivo theragnostic promises of Py-BPy$^{+\bullet}$-COF/PEG by photoacoustic imaging, thermal imaging (Figure 8B) and tumor growth inhibition study using A549 tumor-bearing nude mice. The photoacoustic imaging of A549 tumor indicates maximum accumulation of Py-BPy$^{+\bullet}$-COF/PEG at 4 h post i.v. administration whereas the thermal imaging of A549 tumor-bearing nude mice using an 808 nm laser reveals rapid elevation of

ADVANCED
SCIENCE NEWS
www.advancedsciencenews.com

ADVANCED
FUNCTIONAL
MATERIALS
www.afm-journal.de

temperature from 31 to 67.1 °C supporting remarkable photo-thermal performance of this 2D COF based photothermal agent leading to eradication of tumor burden in nude mice. Thus, the columnar arrays of π-electron present in uniaxially stacked 2D COF layers attributes toward developing a COF-based photothermal agent.

Nanoscale 2D COFs are also being explored for combination therapy of cancer. For instance, Wang et al. have reported an amphiphilic NIR-dye (cyanine) mediated aqueous phase exfoliation of a boronate ester based 2D COF to produce COF–cyanine nanocomposite namely, COF@IR783 (size ≈250 nm), which shows a sharp rise in temperature of water once irradiated with 808 nm laser.[121] This photothermal effect of COF–cyanine nanocomposite in combination with cytotoxic effect of doxorubicin prodrug loaded in the 2D porous network synergistically inhibits the growth of human breast tumor xenografted in nude mice. Similarly, Dong and co-workers have developed a 2D COF-based nanocomposite namely, VONc@COF-Por (3) by simultaneously immobilizing a photosensitizer (PS) and a photothermal agent (PA) onto COF to explore its potential for combinatorial PDT and PTT.[122] The porphyrinic PS is covalently grafted with the 2D COF via bonding defect functionalization whereas the naphthalocyanine (PA) is non-covalently loaded into 2D COF via π–π interaction. Upon photoirradiation with visible red light or NIR (808 nm), VONc@COF-Por (3) exhibited high ROS generation and ≈56% of photothermal conversion leading to a notable combined PDT/PTT efficacy in inhibiting growth of MCF-7 cells under in vitro and in vivo settings.

Inorganic nanoparticles based photosensitizer in combination with nanoscale 2D COFs are also being explored in combined phototherapy of cancer. For instance, Pang and co-workers have reported two composite nanomaterials namely, PEGylated COF-LZU-1-CuSe[123] and hyarulonic acid functionalized COF-LZU-1-Ag$_2$Se[124] derived from an amine based 2D COF (COF-LZU-1) in combination with inorganic photothermal agents CuSe and Ag$_2$Se, respectively, and explored their efficacy for combined PDT and PTT using in vivo tumor model of HeLa cells. Only 2D COF can also exhibit combined PDT and PTT. Wang et al. have reported that efficient molecular packing as well as large surface area in nanoscale (≈100 nm) porphyrin-based 2D COF namely, COF-366, enables impressive combinatorial phototherapy as well as photoacoustic (PA) imaging leading to a significant tumor growth inhibition and its convenient monitoring in mouse model of breast cancer.[125]

Collectively, nanoscale 2D COFs, although the field is in its infancy, have started to show initial promises in drug delivery and phototherapy especially in terms of high loading efficiency, sustained release of payloads and impressive photoelectric property. Biocompatible polymer, liposomes, and inorganic nanoparticles have been well studied as potential drug carriers. However, suboptimal drug loading efficiency, unpredictable drug release behavior, and lack of tunable surface functionality are possibly the major reasons limiting their therapeutic efficacy. To this end, materials with ordered porosity including 2D COF show excellent drug loading efficiency and predictable drug release behavior due to their well-ordered porous structure. Tunable pores of 2D COF in terms of pore size, geometry, and functionalities also offer ample scope of controlling drug loading/release based on desirable host–guest interaction. Furthermore, their tailorable surface functionality adds to the targeting ability indicating their future promises as a drug carrier.

5.3. Biosensing and Bioimaging

The excellent photoelectrical properties of 2D COFs due to the extended π-conjugated system and a great scope of hydrogen bonding with biomolecules have triggered researchers intriguing their potential as a biosensor (Table 3). In 2014, Wang et al. have first demonstrated construction of an imine-based COFs thin film on amine-functionalized silicon substrate for electrochemical based detection of BSA protein and DNA in aqueous solution.[126] Upon electrolysis, the biomolecules get absorbed on the imine populated 2D COF thin film surface via electrolytic interaction. This absorption, unlike normal surface phenomena, rather improves the electrochemical activity of the biomolecules–COF thin films composite leading to declining in simulated charge-transfer resistance (R_{ct}) value measured via electrochemical impedance spectroscopy (EIS). Thus, EIS based estimation of decline in R_{ct} value enables detection of BSA protein or DNA in aqueous solution using the aforementioned 2D COF thin film. However, low sensitivity, strong background noise, as well as lack of a specific recognition moiety are the major factors limiting the efficiency of COF-based electrochemical sensing. To improve the sensing efficacy of 2D COF

Table 3. 2D-COF in biosensing.

Method of sensing	COF name	Linkage	Sensing	Detection limit	Year	Refs.
Electrochemical	Imine based 2D-COF thin film on Si surface	Imine	BSA protein and DNA in aqueous solution	Not mentioned	2014	[126]
	p-COF	Imine	EGFR specific aptasensor	5.64 fg mL^{-1}	2019	[127]
	Py-M-COF	Imine	Aptasensor for detection of enrofloxacin and ampicillin	6.07 and 0.04 fg mL^{-1}, respectively	2019	[128]
	Co-MOF@TPN-COF	Imine	Aptasensor for detection of ampicillin	0.217 fg mL^{-1}	2019	[129]
Fluorescence	TPA-COF	Imine	Single strand DNA	20×10^{-12} M	2017	[75]
	TpTta	β-ketoenamine	Single strand DNA & nucleotides	3.7×10^{-12} M	2017	[131]
	EB-TFB	β-ketoenamine	Label-free detection of double strand DNA	Not mentioned	2018	[24f]

based, Yan et al. have recently developed a porphyrin-based 2D COF immobilizing aptamer on their surface and explored it as lab electrochemical aptasensor for detection of EGFR or EGFR positive cancer cells.[127] The 2D COF is synthesized from condensation of terphthaldehyde and 5,10,15,20-tetrakis(4-aminophenyl)porphyrin as precursor monomers. The rich π-conjugation of porphyrin-based frameworks allows excellent electrochemical signal via π–π stacking interaction with aptamer while the aptamer enables selective detection of EGFR and thereby, increases the sensitivity of detection. Thus, the biorecognition based interaction between the EGFR or EGFR positive cells and aptamer strands decreases electrochemical response of the aptamer-COF, which can be monitored by EIS and thereby providing a tool for biosensing EGFR or cancer cells expressing EGFR. This aptamer-COF possesses specific surface area (BET) of 117.2 m^2 g^{-1} and exhibits an ultrasensitive detection of EGFR over a broad linear range (0.05–100 pg mL^{-1}) with a low detection limit (LOD) as low as of 5.64 fg mL^{-1} (as measured via differential pulse voltammetry) or 7.54 fg mL^{-1} (as measured via EIS). As biosensing by the 2D material is initiated by adsorption, a surface phenomenon, surface area of these 2D materials plays a crucial role in determining the efficacy of biosensing. Recently, Wang et al. have also reported development of another porphyrin-based 2D COF comprising of melamine and 1,3,6,8-tetrakis (4-formyl phenyl) pyrene building units as electrochemical aptasensor for detection of antibiotics enrofloxacin (ENR) and ampicillin (AMP).[128] High BET surface area (495.5 m^2 g^{-1}) along with the extended π-conjugation throughout porphyrin-based 2D COF enables ultrasensitive detection of the antibiotics with LOD value of 6.07 fg mL^{-1} for enrofloxacin and that of 0.04 fg mL^{-1} for ampicillin. Recently, Liu et al. have also reported a 2D MOF–COF nanocomposite (comprising of cobalt-based MOF and triazine based COF) as ultrasensitive electrochemical aptasensor for detection of ampicillin.[129] Authors have demonstrated that it shows an extremely low LOD value of 0.217 fg mL^{-1} for AMP within a detection range varying from 0.001 to 2000 pg mL^{-1} and can determine the presence of AMP residue in river water, human serum as well as in milk. However, the mechanism of synergistically enhanced biosensing activity of this 2D COF-MOF composite compared to only 2D COF or MOF component is not clearly mentioned.

Fluorescence method based biosensing has also been studied using 2D COFs. For instance, Zhang et al. have reported the synthesis of an imine based 2D COF, namely, TPA-COF synthesized from equimolar mixture of flexible building blocks 1,3,5-tris(4-aminophenyl)amine and 1,3,5-tris(4-formyl phenyl)amine.[75] TPA–COF has a morphology of hexagonal sheet-like structure stacked in layers as confirmed by SEM and TEM (**Figure 9**A). The flexibility of building blocks loosens the interlayer stacking favoring exfoliation of the 2D TPA–COF to the ultrathin (3.5 ± 0.3 nm) nanosheets (NS). These ultrathin nanosheet of TPA–COF (TPA–COF–NS) possess high specific surface area (BET) of 1136.5 m^2 g^{-1}, which can be explored as a fluorescence-based sensing platform for DNA detection. To establish it, they have designed two hairpin DNA probes H1 and H2 in such a way that combination of H1 & H2 sequence is complementary to that of the target DNA and one of the DNA probes (e.g., H1) is

fluorescently tagged. H1 & H2 easily absorbed on TPA–COF–NS surface via π-stacking interactions leading to fluorescence resonance energy transfer (FRET) resulting in fluorescence quenching of the dye attached to H1. However, in presence of the target DNA, a specific hybridization chain reaction is triggered among H1 and H2,[130] resulting in formation of the long double-stranded DNA (dsDNA), which further gets detached from the TPA–COF–NS surface due to diminished π–π stacking interaction eventually leading to the recovery of fluorescence. The extent of fluorescence recovery in the presence of target DNA compared to blank control (TPA–COF NSs with H1 and H2) determines the sensing efficacy. TPA–COF–NSs exhibit high sensitivity toward single-stranded DNA with a LOD value of 20×10^{-12} M in the linear range of 0–1×10^{-9} M. Thus, like other 2D nanomaterials, 2D COF nanosheets can also be used for DNA sensing platform. In the same year, Yan et al. have also reported a ketoenamine based 2D COF (TpTta) as similar fluorescence-based biosensing platform for detection of nucleotides and single-stranded DNA.[131] TpTta possesses a BET area of 609 m^2 g^{-1}, works based on similar fluorescence quenching principle and exhibits a LOD value of 3.7×10^{-9} M toward single-stranded DNA. Facile adsorption of biomolecules onto TpTta surface through H-bonding ability as well as π–π stacking interaction with biomolecules are believed to be the contributing factors to the high sensitivity of biosensing. The difference in LOD values of the two 2D COF-based biosensors further confirms that large specific surface area and ultra-thinness of 2D materials are essential for ultrasensitive biosensing.

Toward developing biosensing platform for double-stranded DNA (dsDNA), Ajayaghosh et al. demonstrated an interesting strategy of exploring ethidium bromide based 2D ionic covalent organic nanosheets namely, EB-TFP-iCONs (Figure 9B).[24f] In aqueous medium EB-TFP-iCONs spontaneously reassemble into ordered 2D stacks and incorporate dsDNA inside to form hybrid crystalline nanosheets EB-TFP-iCONs-DNA resulting in enhancement of fluorescence intensity at 600 nm. This 2D COF DNA hybrid nanosheets formation is specific to dsDNA as single-stranded DNA weakly interacts with EB-TFP-iCONs and fails to reassemble the exfoliated nanosheets of EB-TFP-iCONs. Notably, this is the first report of 2D COF acting as a label-free biosensor for fluorescence-based detection of double-stranded DNA.

2D COF nanosheets have also been explored as a potential theragnostic platform for bioimaging. Recently, Das et al. have reported microwave-assisted synthesis of a triazine-based COF, which gains photoluminescence properties by six times with a blue shift (compared to bulk form) upon exfoliation in water (**Figure 10**A–C).[132] High-resolution TEM confirms that exfoliated TTA–DFP COF has nanosheet like morphology with a size of ≈22 nm comprising of about four stacked layers with a net topological height profile of ≈1.5 nm as confirmed by AFM. This TTA–DFP COF nanosheets (TTA–DFP CONs) has been explored for nuclear staining in HeLa cells. The authors have demonstrated that this triazine-based acid stable TTA–DFP CONs enter into HeLa cells via clathrin-mediated endocytosis within 30 min, selectively accumulate in the nucleus to stain it without hampering cellular integrity (Figure 10C) and therefore, may find their application as a potential biosensor for nuclear imaging.
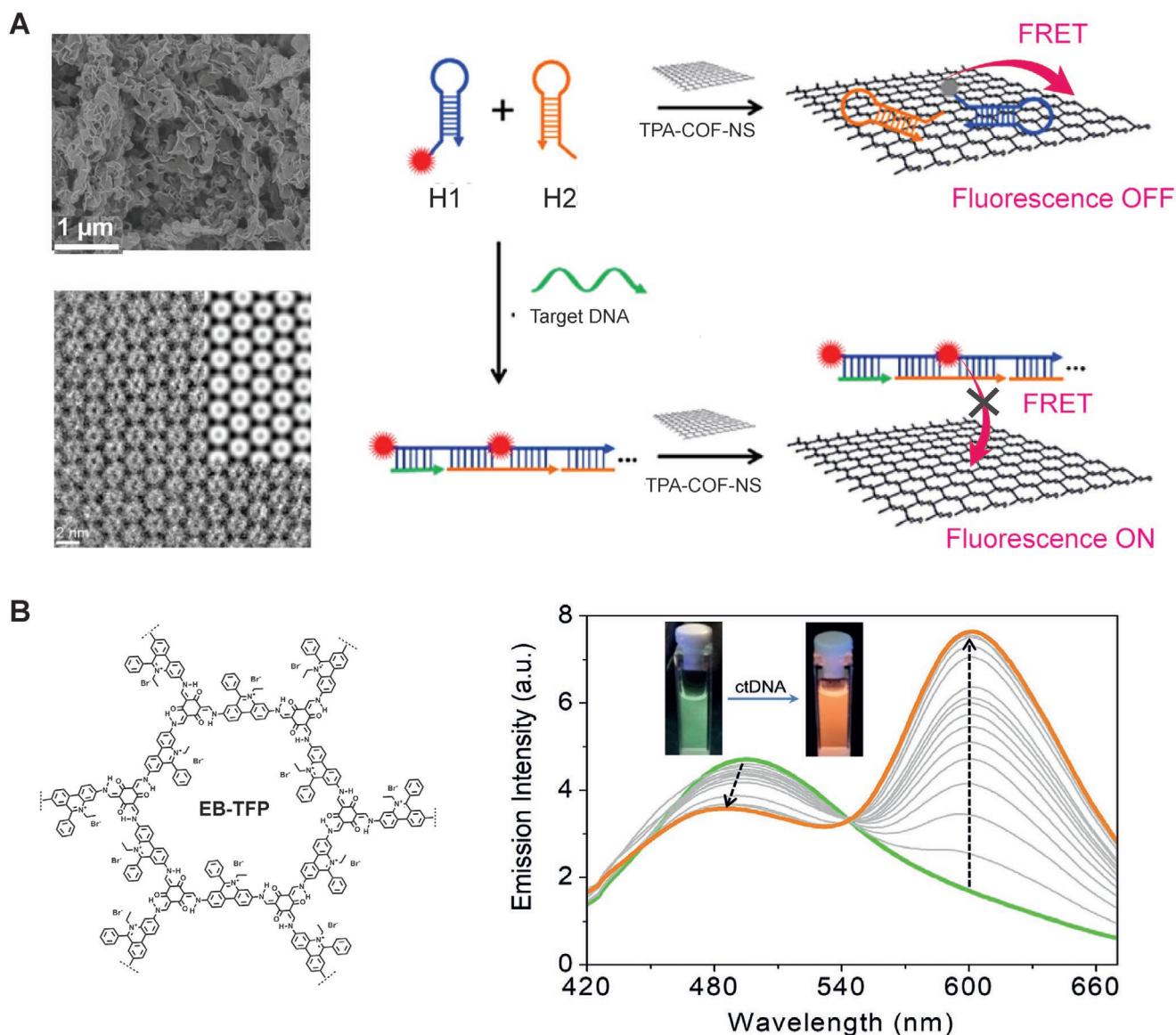
Figure 9. Nanosheets of 2D COF in fluorescence-based biosensing for DNA detection. A) Ultrathin nanosheets of an imine-based 2D COF, namely, TPA-COF-NS can act as fluorescence-based sensor for detection of single stranded DNA SEM and TEM of TPA-COF-NS. Principle of fluorescence-based DNA detection using nanosheets of 2D COFs: In absence of target DNA, hairpin DNA probes H1(fluorescence-tagged) and H2 are adsorbed on surface of TPA-COF-NS leading to fluorescence quenching via FRET, whereas in presence of the target DNA a specific hybridization chain reaction is triggered producing the long double-stranded DNA (dsDNA) which further gets detached from the TPA-COF-NS surface resulting in recovery of fluorescence. Adapted with permission.[75] Copyright 2017, American Chemical Society. B) Chemical structure of an imine-based 2D COF containing ethidium bromide as molecular building blocks, namely EB-TFP, for label-free detection of double-stranded (ds) DNA. Significant enhancement of fluorescence intensity of EB-TFP in presence of ds DNA enables fluorescence-based label-free biosensing of ds DNA. Adapted with permission.[24f] Copyright 2018, Wiley-VCH.

2D COF can also act as a host system for bioimaging. In 2018, Zhang and co-workers reported development of a fluorescent COF nanoprobe, namely TpASH–NPHS, for intracellular enzymes resistant detection of endogenous hydrogen sulfide (H_2S).[133] TpASH–NPHS consisting of imine-based COF TpASH (Figure 7C) functionalize with "two-photon fluorescent probe" 4-amino-1,8-naphthalimide derivative (NPHS) forms 2D nanosheets (with a diameter of ≈90 nm and a thickness of ≈1.6 nm) upon solvent-assisted exfoliation from its bulk form. In presence of H_2S, the azide group of NPHS part undergoes reduction to amine leading to much enhancement of fluorescent intensity. Importantly, unlike small-molecule fluorescent probe (e.g., only NPHS) which are easily accessible by the intracellular reductase enzyme the 2D cage structure of TpASH–NPHS COF can sequester the NPHS part from enzyme attack while retaining their activity for H_2S sensing. Authors have demonstrated the potential of TpASH–NPHS COF as a potent fluorescent-based biosensor for selective detection of H_2S in a range of samples including live cell, deep tumor tissue as well as in a mouse model of cirrhosis.
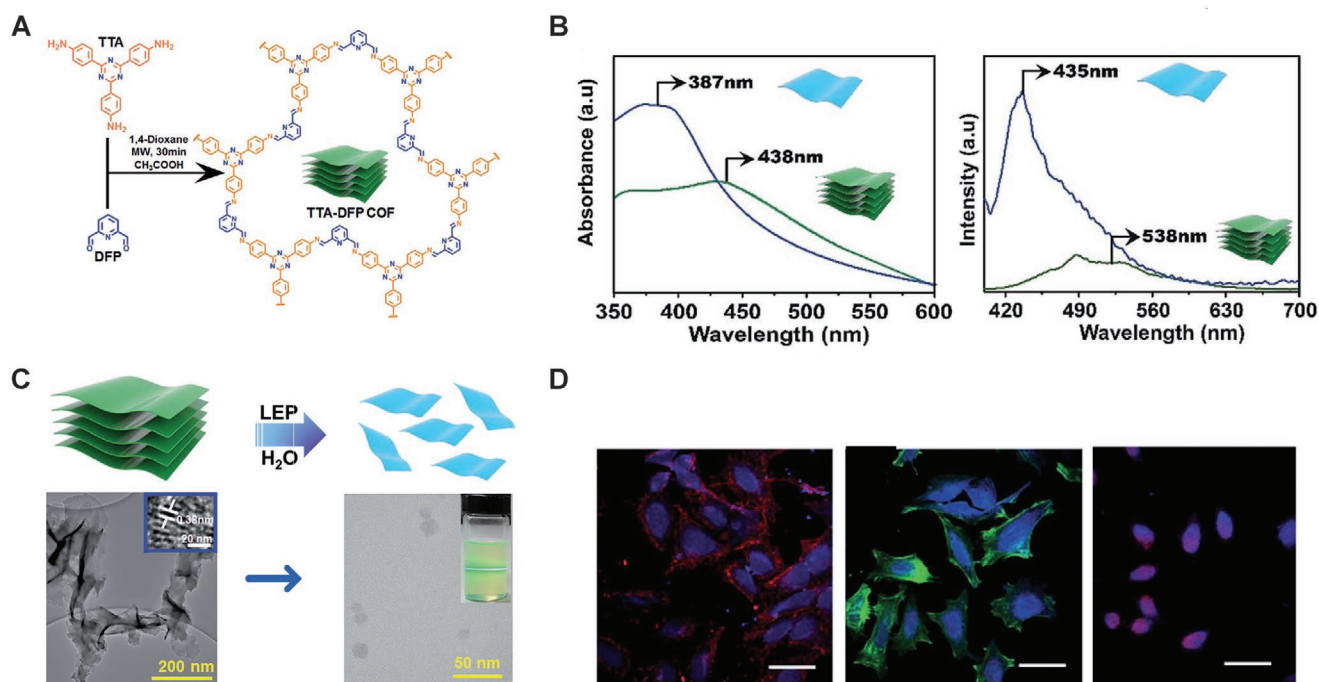
Figure 10. 2D COF for bioimaging. A) TTA–DFP COF, a triazine-based 2D COF formed via condensation of TTA and DFP B) gains photoluminescence properties with a blue-shift upon exfoliation in water. C) TEM of bulk (left panel) and nanosheets (right panel) of TTA–DFP with photoluminescence picture (right panel, inset). D) Confocal images of HeLa cells incubated with exfoliated nanosheets of TTA–DFP and separately treated with: a plasma membrane marker (left image), actin marker (middle image), and nucleus marker (right image) indicating nuclear localization of exfoliated TTA–DFP nanosheets. Adapted with permission.[32] Copyright 2018, Royal Society of Chemistry.
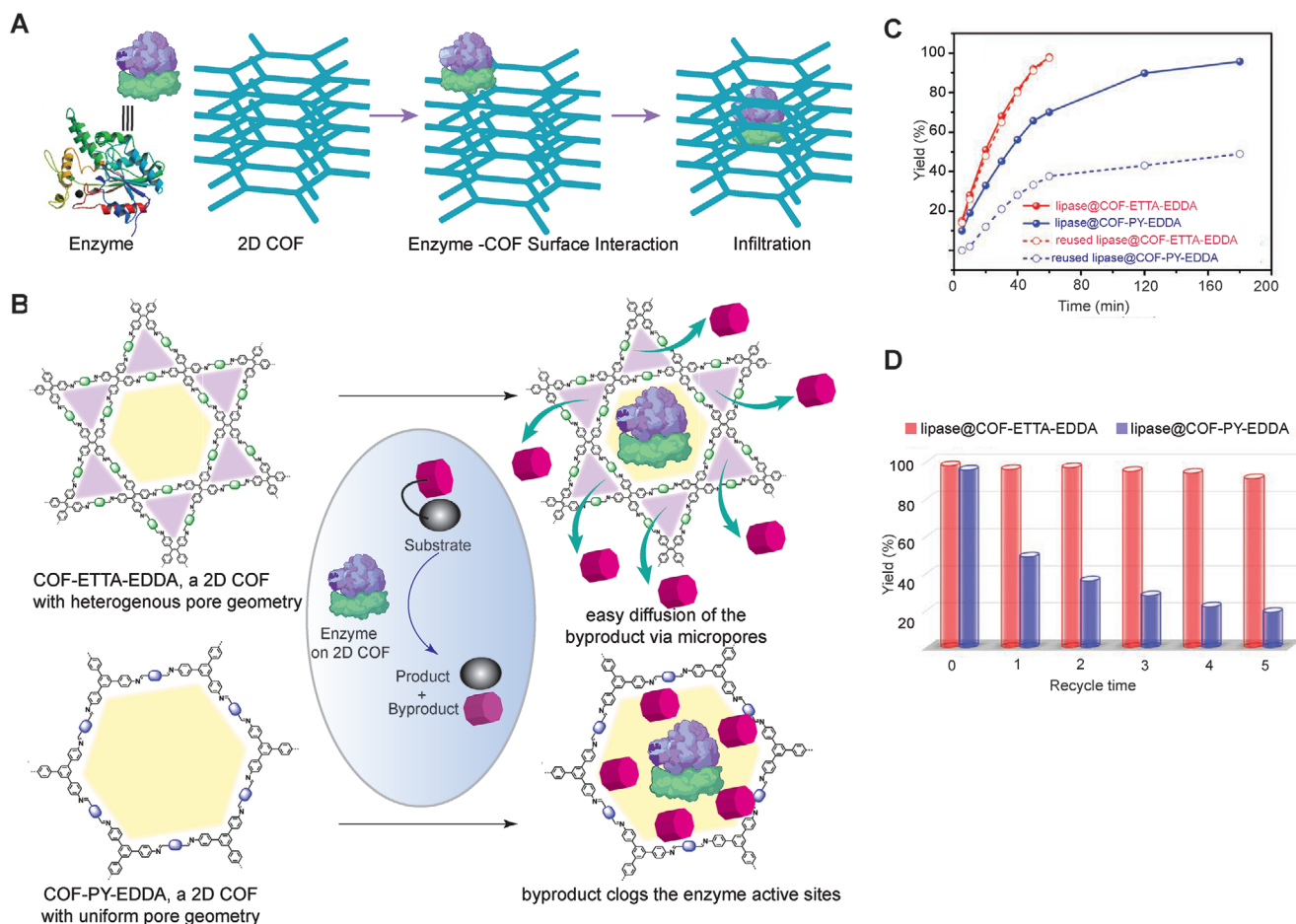
5.4. Biocatalysis

Toward achieving green and sustainable approach of large-scale chemical production biocatalysts has attracted significant attention in recent years. However, the lack of recyclability and sustainable operational stability often limits their practical implementation. Porous materials, including zeolites, celite, mesoporous silica, MOF and COF are being investigated as a molecular flask for storage of some enzymes. Recently, Sun et al. have reported an interesting study of exploring imine based 2D COF as a biomolecular flask for enzyme immobilization.[134] Authors have used COF-OMe, prepared from condensation of 1,3,5-tris(4-aminophenyl)-benzene and dimethoxy terephthaldehyde as initial precursor material. The mesoporous (1D) channel of COF–OMe with 3.3 nm pore size can effectively immobilize Amano lipase PS, an enzyme with a similar small-axis length ($\approx$3.2 nm) (**Figure 11**A) while preserving its activity. Authors have demonstrated that the enzyme COF biocomposite (COF–OMe–PS) outperforms free enzyme as well as other biocomposites made from other types of porous materials, including metal–organic framework and mesoporous silica in catalytic activities. They have also demonstrated that the activity of such host immobilized enzymes can be modulated via tuning the pore microenvironment of host COFs by varying inner pore wall functionalities while maintaining the same reticular chemistry.

To further improve the enzymatic activity, durability, and recyclability of the biocatalyst (enzyme COF biocomposite) the same group has reported an interesting strategy of using hierarchically porous 2D COF as host material for enzyme immobilization.[135] The authors have developed a star shape 2D COFs with dual-pores, namely COF–ETTA–EDDA, containing large hexagonal mesopores at core (pore diameter of $\approx$3.98 nm) surrounded by triangular micropores (Figure 11). In an enzyme-catalyzed transesterification reaction, the dual-pores 2D COFs show much higher enzymatic activity (Figure 11C) and recyclability (Figure 11D) compared with the corresponding single pore analogue, namely COF-PY-EDDA (Figure 11). The better performance of hierarchically porous 2D COF is presumably mediated via active diffusion of the byproducts through the narrow pores and thereby avoiding clogging of enzyme active sites while the large pores are engaged in preserving the enzymes after each catalytic cycle. Pore wall modification of host COF can strongly influence the adsorption performance toward guest molecules. Recently, Lohse et al. have also reported the synthesis of β-ketoenamine based 2D COFs, namely, (TpBD(NH$_2$)$_2$), (TpBD(NO$_2$)$_2$), & TpBD(NHCOCH$_3$)$_2$ and have demonstrated (TpBD(NH$_2$)$_2$) shows the highest capacity for lactic acid storage.[136] Similarly, Samui et al. also explored an amine based 2D COF for storing industrially important enzyme α-amylase.[137]

5.5. Other Biomedical Applications

Besides the applications mentioned above, 2D COFs are also being explored for other biomedical uses. Recently, Banerjee et al. have developed an antibacterial 2D ionic covalent organic

Figure 11. 2D COFs in biocatalysis. A) schematic of enzyme immobilization on 2D COFs,[134] Image are adapted with permission, Copyright 2018, American Chemical Society. B) A hierarchically porous 2D COF containing large hexagonal mesopores at core surrounded by triangular micropores serve as a better platform for enzymatic performance compared to the corresponding 2D COF with uniform hexagonal pores. The triangular micropores in hierarchically porous 2D COF allows active diffusion of the byproduct which facilitates maintaining the active catalytic site and thereby, exhibit C) higher enzymatic (lipase) activity and D) recyclability compared to that of the 2D COF with uniform hexagonal pores. Adapted with permission.[135] Copyright 2019, Wiley-VCH.

nanosheets (2D-iCONs) of thickness ≈2–5 nm via introducing guanidinium halide in the backbone of 2D-COF (**Figure 12**).[24c] Wise selection of cationic guanidinium moiety not only imparts antimicrobial property in 2D-iCONs via rupturing negatively charged phospholipid based bacterial cell membrane but also facilitates its exfoliation in water. Authors have demonstrated that this guanidinium chloride-based 2D-iCONs can significantly reduce colony formation of both Gram-negative and Gram-positive bacteria in a dose-dependent manner individually and also as additive with matrix membrane indicating their potential use in antimicrobial coatings of biomedical devices. The bacterial growth on surface can also be controlled using reversible exfoliation-restacking of 2D COFs. Recently, Mal et al. have developed a propidium iodide based 2D-iCONs, which efficiently inhibit bacterial growth once exfoliated while chemical mediated restacking of the nanosheets switch to loss of their antibacterial activity, which can further be regenerated by removing the chemical providing a control over bacterial growth.[24e] Other sets of antibacterial 2D COFs are reported by Liu et al. which can kill bacteria in presence of light.[138] Authors have demonstrated that 100 µg L^{-1} of these two 2D COFs can kill 90% of bacteria when illuminated with light for 60–90 min.

6. Conclusion and Outlooks

In this article, we have described a comprehensive overview of different 2D COFs, which are relevant for biomedical application. These porous organic polymeric material (2D COFs) possess several advantages including biodegradability, large and accessible pores, high surface area, ordered structure, as well as the tailorable surface, which are highly beneficial for biomedical application. Furthermore, the large surface area along with the high π-electron density of 2D COFs makes them an excellent candidate for biosensing and bioimaging. The good electrical conductivity of porphyrin based 2D COFs may trigger researchers investigating their potentials in tissue engineering, especially for neural or cardiac tissue engineering. However, in spite of these advantages, 2D COFs suffer from many
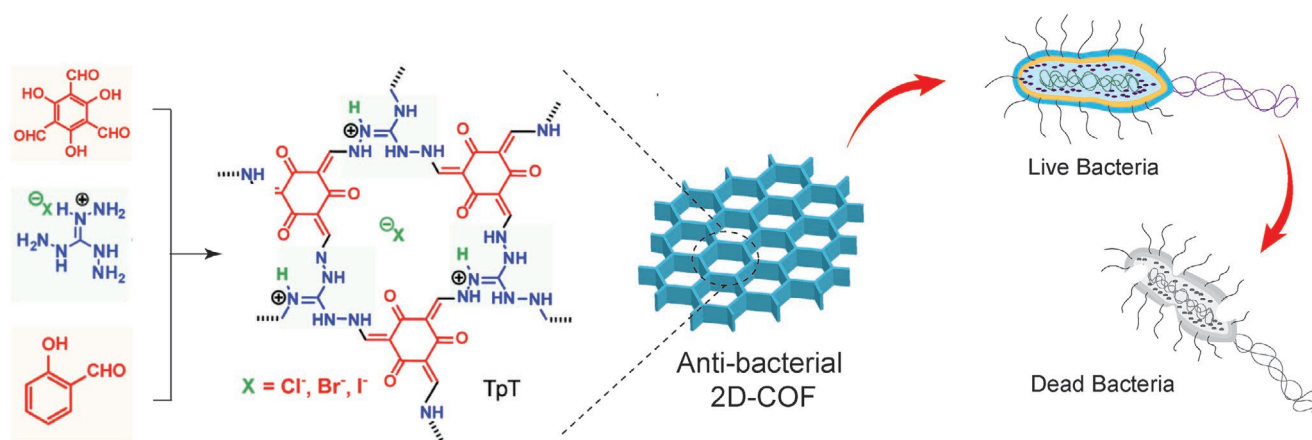
Figure 12. Guanidinium halide based 2D COF nanosheets for antibacterial coating of biomedical devices. The positively charged guanidinium halide moiety ruptures the negatively charged phospholipid based bacterial cell membrane and thereby shows antimicrobial property. Structure of nanosheets (iCONs) was adapted with permission.[24c] Copyright 2016, American Chemical Society.

limitations and therefore translation of these nanomaterials from "bench to bedside" will need detail analysis.

The major limitations of the 2D COFs holding their practical implementations are poor physiological stability and scalability. Being composed of building blocks which are mostly polycyclic aromatic derivatives water dispersibility of the 2D COFs is poor compared to other porous materials including polymers and mesoporous silica nanoparticle. Furthermore, reversible nature of the linkages forming 2D COFs which adds to its biodegradability also, on the other hand, imparts vulnerability toward humid, acidic and alkaline environments. The poor stability of 2D COFs can lead to limited shelf life for biomedical use. It is worth mentioning that significant efforts are focused toward improving their physiological stability as well as developing robust 2D COFs, which are stable in harsh condition. Another concern with 2D COF is the difficulty in large scale production and batch-to-batch reproducibility. Due to complex molecular arrangements (e.g., different types of layer stacking, different pore arrangements, etc.) within the 2D COFs structure, it is challenging to produce uniform size in different batches. Therefore, it is necessary to develop a simple and effective method to achieve scalability, uniformity, and reproducibility in producing 2D COF. Similarly, due to the complexity in pore structure and pore arrangements within 2D COF, it is also crucial to study drug loading and release pattern of 2D COF carefully toward achieving uniformity and reliability as a drug carrier.

Moreover, biosafety profiles of COFs are not yet investigated in detail. So far, only some preliminary in vitro studies are in the literature mostly focusing on determining cellular cytotoxicity of 2D COFs. As covalent organic frameworks are a new class of nanomaterials it is important to thoroughly examine their hemocompatibility, histocompatibility, cytotoxicity, and neurotoxicity especially when the degradation product of 2D COFs are polycyclic aromatic compounds. So far, only one report has demonstrated the use of 2D COF based material for in vivo drug delivery. A thorough evaluation of in vivo systemic toxicity including immunogenicity both in short-term exposure and long-term exposure needs to be done in a small animal model before their pharmaceutical application.

Overall, 2D COFs is the latest member of porous crystalline polymeric material with abundant voids. In recent years researches on 2D COF are mostly focusing on the development of new linkage motifs & building blocks to improve chemical stability, pore space, and geometry as well as improving synthetic strategy to achieve scalability. Researches on the potential application of 2D COF has just begun showing initial promise. In the future, it may open new doors for exciting opportunities to advance human healthcare.

Conflict of Interest

The authors declare no conflict of interest.

Author Contributions

The manuscript was written through contributions of all authors. All authors have given approval to the final version of the manuscript.

[1] a) A. G. Slater, A. I. Cooper, *Science* **2015**, *348*, aaa8075; b) C. S. Diercks, O. M. Yaghi, *Science* **2017**, *355*, eaal1585.

[2] M. E. Hailian Li, M. O'Keeffe, O. M. Yaghi, *Nature* **1999**, *402*, 276.

[3] a) Z. R. Herm, E. D. Bloch, J. R. Long, *Chem. Mater.* **2014**, *26*, 323; b) K.-J. Chen, D. G. Madden, S. Mukherjee, T. Pham, K. A. Forrest, A. Kumar, B. Space, J. Kong, Q.-Y. Zhang, M. J. Zaworotko, *Science* **2019**, *366*, 241; c) X. Cui, K. Chen, H. Xing, Q. Yang, R. Krishna, Z. Bao, H. Wu, W. Zhou, X. Dong, Y. Han, B. Li, Q. Ren, M. J. Zaworotko, B. Chen, *Science* **2016**, *353*, 141.

[4] A. P. Côté, A. I. Benin, N. W. Ockwig, M. Keeffe, A. J. Matzger, O. M. Yaghi, *Science* **2005**, *310*, 1166.

[5] a) Z. Wang, S. Zhang, Y. Chen, Z. Zhang, S. Ma, *Chem. Soc. Rev.* **2020**, *49*, 708; b) N. Huang, X. Chen, R. Krishna, D. Jiang, *Angew. Chem., Int. Ed.* **2015**, *54*, 2986; c) Y. Zeng, R. Zou, Y. Zhao, *Adv. Mater.* **2016**, *28*, 2855; d) J. Lv, Y.-X. Tan, J. Xie, R. Yang, M. Yu, S. Sun, M.-D. Li, D. Yuan, Y. Wang, *Angew. Chem., Int. Ed.* **2018**, *57*, 12716.

[6] R. W. Tilford, S. J. Mugavero Iii, P. J. Pellechia, J. J. Lavigne, *Adv. Mater.* **2008**, *20*, 2741.

[7] a) A. Halder, S. Karak, M. Addicoat, S. Bera, A. Chakraborty, S. H. Kunjattu, P. Pachfule, T. Heine, R. Banerjee, *Angew. Chem., Int. Ed.* **2018**, *57*, 5797; b) X. Li, C. Zhang, S. Cai, X. Lei, V. Altoe, F. Hong, J. J. Urban, J. Ciston, E. M. Chan, Y. Liu, *Nat. Commun.* **2018**, *9*, 2998; c) L. Li, F. Lu, R. Xue, B. Ma, Q. Li, N. Wu, H. Liu, W. Yao, H. Guo, W. Yang, *ACS Appl. Mater. Interfaces* **2019**, *11*, 26355.

[8] H. Xu, S. Tao, D. Jiang, *Nat. Mater.* **2016**, *15*, 722.

[9] J. Zhang, X. Han, X. Wu, Y. Liu, Y. Cui, *J. Am. Chem. Soc.* **2017**, *139*, 8277.

[10] a) F. J. Uribe-Romo, J. R. Hunt, H. Furukawa, C. Klöck, M. O'Keeffe, O. M. Yaghi, *J. Am. Chem. Soc.* **2009**, *131*, 4570; b) C. J. Doonan, D. J. Tranchemontagne, T. G. Glover, J. R. Hunt, O. M. Yaghi, *Nat. Chem.* **2010**, *2*, 235; c) H. Furukawa, O. M. Yaghi, *J. Am. Chem. Soc.* **2009**, *131*, 8875.

[11] a) Q. Sun, Z. Dai, X. Meng, F.-S. Xiao, *Chem. Soc. Rev.* **2015**, *44*, 6018; b) X. Wang, X. Han, J. Zhang, X. Wu, Y. Liu, Y. Cui, *J. Am. Chem. Soc.* **2016**, *138*, 12332; c) F. R. Fortea-Pérez, M. Mon, J. Ferrando-Soria, M. Boronat, A. Leyva-Pérez, A. Corma, J. M. Herrera, D. Osadchii, J. Gascon, D. Armentano, E. Pardo, *Nat. Mater.* **2017**, *16*, 760.

[12] a) V. Stavila, A. A. Talin, M. D. Allendorf, *Chem. Soc. Rev.* **2014**, *43*, 5994; b) B. Sun, C.-H. Zhu, Y. Liu, C. Wang, L.-J. Wan, D. Wang, *Chem. Mater.* **2017**, *29*, 4367; c) G. Lin, H. Ding, D. Yuan, B. Wang, C. Wang, *J. Am. Chem. Soc.* **2016**, *138*, 3302.

[13] M.-X. Wu, Y.-W. Yang, *Adv. Mater.* **2017**, *29*, 1606134.

[14] a) R. Liu, T. Yu, Z. Shi, Z. Wang, *Int. J. Nanomed.* **2016**, *11*, 1187; b) X. Du, S. Z. Qiao, *Small* **2015**, *11*, 392.

[15] S. Das, P. Heasman, T. Ben, S. Qiu, *Chem. Rev.* **2017**, *117*, 1515.

[16] R. Dawson, A. I. Cooper, D. J. Adams, *Prog. Polym. Sci.* **2012**, *37*, 530.

[17] A. M. Evans, L. R. Parent, N. C. Flanders, R. P. Bisbey, E. Vitaku, M. S. Kirschner, R. D. Schaller, L. X. Chen, N. C. Gianneschi, W. R. Dichtel, *Science* **2018**, *361*, 52.

[18] a) G. Zhang, M. Tsujimoto, D. Packwood, N. T. Duong, Y. Nishiyama, K. Kadota, S. Kitagawa, S. Horike, *J. Am. Chem. Soc.* **2018**, *140*, 2602; b) Z.-F. Pang, T.-Y. Zhou, R.-R. Liang, Q.-Y. Qi, X. Zhao, *Chem. Sci.* **2017**, *8*, 3866.

[19] S. Sant, V. Nadeau, P. Hildgen, *J. Controlled Release* **2005**, *107*, 203.

[20] a) C. Tamames-Tabar, D. Cunha, E. Imbuluzqueta, F. Ragon, C. Serre, M. J. Blanco-Prieto, P. Horcajada, *J. Mater. Chem. B* **2014**, *2*, 262; b) C. F. W. Marcus Hoop, R. Riccò, F. Mushtaq, A. Terzopoulou, X. Z. Chen, A. J. deMello, C. J. Doonan, P. Falcaro, B. J. Nelson, J. Puigmartí-Luis, S. Pané, *Appl. Mater. Today* **2018**, *11*, 13.

[21] a) H. M. El-Kaderi, J. R. Hunt, J. L. Mendoza-Cortés, A. P. Côté, R. E. Taylor, M. Keeffe, O. M. Yaghi, *Science* **2007**, *316*, 268; b) S. Yan, X. Guan, H. Li, D. Li, M. Xue, Y. Yan, V. Valtchev, S. Qiu, Q. Fang, *J. Am. Chem. Soc.* **2019**, *141*, 2920; c) X. Ma, T. F. Scott, *Commun. Chem.* **2018**, *1*, 98.

[22] R. Mercado, R.-S. Fu, A. V. Yakutovich, L. Talirz, M. Haranczyk, B. Smit, *Chem. Mater.* **2018**, *30*, 5069.

[23] a) Y.-B. Zhang, J. Su, H. Furukawa, Y. Yun, F. Gándara, A. Duong, X. Zou, O. M. Yaghi, *J. Am. Chem. Soc.* **2013**, *135*, 16336; b) D. N. Bunck, W. R. Dichtel, *Angew. Chem., Int. Ed.* **2012**, *51*, 1885.

[24] a) S. Chandra, S. Kandambeth, B. P. Biswal, B. Lukose, S. M. Kunjir, M. Chaudhary, R. Babarao, T. Heine, R. Banerjee, *J. Am. Chem. Soc.* **2013**, *135*, 17853; b) S. Mitra, H. S. Sasmal, T. Kundu, S. Kandambeth, K. Illath, D. Díaz Díaz, R. Banerjee, *J. Am. Chem. Soc.* **2017**, *139*, 4513; c) S. Mitra, S. Kandambeth, B. P. Biswal, A. Khayum M, C. K. Choudhury, M. Mehta, G. Kaur, S. Banerjee, A. Prabhune, S. Verma, S. Roy, U. K. Kharul, R. Banerjee, *J. Am. Chem. Soc.* **2016**, *138*, 2823; d) M. A. Khayum, S. Kandambeth, S. Mitra, S. B. Nair, A. Das, S. S. Nagane, R. Mukherjee, R. Banerjee, *Angew. Chem., Int. Ed.* **2016**, *55*, 15604; e) A. Mal, S. Vijayakumar, R. K. Mishra, J. Jacob, R. S. Pillai, B. S. Dileep Kumar, A. Ajayaghosh, *Angew. Chem.* **2019**, https://doi.org/10.1002/ange.201912363; f) A. Mal, R. K. Mishra, V. K. Praveen, M. A. Khayum, R. Banerjee, A. Ajayaghosh, *Angew. Chem., Int. Ed.* **2018**, *57*, 8443.

[25] a) P. Tao, S. Yao, F. Liu, B. Wang, F. Huang, M. Wang, *J. Mater. Chem. A* **2019**, *7*, 23512; b) C. Tan, X. Cao, X.-J. Wu, Q. He, J. Yang, X. Zhang, J. Chen, W. Zhao, S. Han, G.-H. Nam, M. Sindoro, H. Zhang, *Chem. Rev.* **2017**, *117*, 6225.

[26] Y. Luo, Z. Li, C. Zhu, X. Cai, L. Qu, D. Du, Y. Lin, *Trends Biotechnol.* **2018**, *36*, 1145.

[27] a) F. Zhao, H. Liu, D. S. Mathe, A. Dong, J. Zhang, *Nanomaterials* **2018**, *8*, 15; b) M. S. Lohse, T. Bein, *Adv. Funct. Mater.* **2018**, *28*, 1705553; c) H. Wang, Z. Zeng, P. Xu, L. Li, G. Zeng, R. Xiao, Z. Tang, D. Huang, L. Tang, C. Lai, D. Jiang, Y. Liu, H. Yi, L. Qin, S. Ye, X. Ren, W. Tang, *Chem. Soc. Rev.* **2019**, *48*, 488; d) G. Chedid, A. Yassin, *Nanomaterials* **2018**, *8*, 916; e) Y. Song, Q. Sun, B. Aguila, S. Ma, *Adv. Sci.* **2019**, *6*, 1801410; f) N. Huang, P. Wang, D. Jiang, *Nat. Rev. Mater.* **2016**, *1*, 16068; g) Y. Jin, Y. Hu, W. Zhang, *Nat. Rev. Chem.* **2017**, *1*, 0056.

[28] a) X. Feng, X. Ding, D. Jiang, *Chem. Soc. Rev.* **2012**, *41*, 6010; b) F. Beuerle, B. Gole, *Angew. Chem., Int. Ed.* **2018**, *57*, 4850; c) S.-Y. Ding, W. Wang, *Chem. Soc. Rev.* **2013**, *42*, 548.

[29] B. J. Smith, N. Hwang, A. D. Chavez, J. L. Novotney, W. R. Dichtel, *Chem. Commun.* **2015**, *51*, 7532.

[30] L. M. Lanni, R. W. Tilford, M. Bharathy, J. J. Lavigne, *J. Am. Chem. Soc.* **2011**, *133*, 13975.

[31] Y. Du, D. Calabro, B. Wooler, P. Kortunov, Q. Li, S. Cundy, K. Mao, *Chem. Mater.* **2015**, *27*, 1445.

[32] Y. Du, H. Yang, J. M. Whiteley, S. Wan, Y. Jin, S.-H. Lee, W. Zhang, *Angew. Chem., Int. Ed.* **2016**, *55*, 1737.

[33] S. Wan, F. Gándara, A. Asano, H. Furukawa, A. Saeki, S. K. Dey, L. Liao, M. W. Ambrogio, Y. Y. Botros, X. Duan, S. Seki, J. F. Stoddart, O. M. Yaghi, *Chem. Mater.* **2011**, *23*, 4094.

[34] S.-Y. Ding, J. Gao, Q. Wang, Y. Zhang, W.-G. Song, C.-Y. Su, W. Wang, *J. Am. Chem. Soc.* **2011**, *133*, 19816.

[35] F. J. Uribe-Romo, C. J. Doonan, H. Furukawa, K. Oisaki, O. M. Yaghi, *J. Am. Chem. Soc.* **2011**, *133*, 11478.

[36] S. Kandambeth, A. Mallick, B. Lukose, M. V. Mane, T. Heine, R. Banerjee, *J. Am. Chem. Soc.* **2012**, *134*, 19524.

[37] S. Kandambeth, D. B. Shinde, M. K. Panda, B. Lukose, T. Heine, R. Banerjee, *Angew. Chem., Int. Ed.* **2013**, *52*, 13052.

[38] X. Chen, M. Addicoat, E. Jin, L. Zhai, H. Xu, N. Huang, Z. Guo, L. Liu, S. Irle, D. Jiang, *J. Am. Chem. Soc.* **2015**, *137*, 3241.

[39] C. R. DeBlase, K. E. Silberstein, T.-T. Truong, H. D. Abruña, W. R. Dichtel, *J. Am. Chem. Soc.* **2013**, *135*, 16821.

[40] H. Xu, J. Gao, D. Jiang, *Nat. Chem.* **2015**, *7*, 905.

[41] P. J. Waller, S. J. Lyle, T. M. Osborn Popp, C. S. Diercks, J. A. Reimer, O. M. Yaghi, *J. Am. Chem. Soc.* **2016**, *138*, 15519.

[42] Q. Fang, Z. Zhuang, S. Gu, R. B. Kaspar, J. Zheng, J. Wang, S. Qiu, Y. Yan, *Nat. Commun.* **2014**, *5*, 4503.

[43] S. Dalapati, S. Jin, J. Gao, Y. Xu, A. Nagai, D. Jiang, *J. Am. Chem. Soc.* **2013**, *135*, 17310.

[44] A. Nagai, X. Chen, X. Feng, X. Ding, Z. Guo, D. Jiang, *Angew. Chem., Int. Ed.* **2013**, *52*, 3770.

[45] P. Kuhn, M. Antonietti, A. Thomas, *Angew. Chem., Int. Ed.* **2008**, *47*, 3450.

[46] M. J. Bojdys, J. Jeromenok, A. Thomas, M. Antonietti, *Adv. Mater.* **2010**, *22*, 2202.

[47] S. Ren, M. J. Bojdys, R. Dawson, A. Laybourn, Y. Z. Khimyak, D. J. Adams, A. I. Cooper, *Adv. Mater.* **2012**, *24*, 2357.

[48] E. Jin, M. Asada, Q. Xu, S. Dalapati, M. A. Addicoat, M. A. Brady, H. Xu, T. Nakamura, T. Heine, Q. Chen, D. Jiang, *Science* **2017**, *357*, 673.

[49] H. Lyu, C. S. Diercks, C. Zhu, O. M. Yaghi, *J. Am. Chem. Soc.* **2019**, *141*, 6848.

[50] X. Guan, H. Li, Y. Ma, M. Xue, Q. Fang, Y. Yan, V. Valtchev, S. Qiu, *Nat. Chem.* **2019**, *11*, 587.

[51] K. T. Jackson, T. E. Reich, H. M. El-Kaderi, *Chem. Commun.* **2012**, *48*, 8823.

[52] a) Y. Zeng, R. Zou, Z. Luo, H. Zhang, X. Yao, X. Ma, R. Zou, Y. Zhao, *J. Am. Chem. Soc.* **2015**, *137*, 1020; b) X. Chen, M. Addicoat, E. Jin, H. Xu, T. Hayashi, F. Xu, N. Huang, S. Irle, D. Jiang, *Sci. Rep.* **2015**, *5*, 14650.

[53] T. Faury, S. Clair, M. Abel, F. Dumur, D. Gigmes, L. Porte, *J. Phys. Chem. C* **2012**, *116*, 4819.

[54] J. Thote, H. Barike Aiyappa, R. Rahul Kumar, S. Kandambeth, B. P. Biswal, D. Balaji Shinde, N. Chaki Roy, R. Banerjee, *IUCrJ* **2016**, *3*, 402.

[55] N. L. Campbell, R. Clowes, L. K. Ritchie, A. I. Cooper, *Chem. Mater.* **2009**, *21*, 204.

[56] a) H. Wei, S. Chai, N. Hu, Z. Yang, L. Wei, L. Wang, *Chem. Commun.* **2015**, *51*, 12178; b) E. Vitaku, W. R. Dichtel, *J. Am. Chem. Soc.* **2017**, *139*, 12911.

[57] a) W. Zhang, L.-G. Qiu, Y.-P. Yuan, A.-J. Xie, Y.-H. Shen, J.-F. Zhu, *J. Hazard. Mater.* **2012**, *221–222*, 147; b) J. Ge, J. Xiao, L. Liu, L. Qiu, X. Jiang, *J. Porous Mater.* **2016**, *23*, 791.

[58] B. P. Biswal, S. Chandra, S. Kandambeth, B. Lukose, T. Heine, R. Banerjee, *J. Am. Chem. Soc.* **2013**, *135*, 5328.

[59] Y. Peng, G. Xu, Z. Hu, Y. Cheng, C. Chi, D. Yuan, H. Cheng, D. Zhao, *ACS Appl. Mater. Interfaces* **2016**, *8*, 18505.

[60] S. Karak, S. Kandambeth, B. P. Biswal, H. S. Sasmal, S. Kumar, P. Pachfule, R. Banerjee, *J. Am. Chem. Soc.* **2017**, *139*, 1856.

[61] D. A. Vazquez-Molina, G. S. Mohammad-Pour, C. Lee, M. W. Logan, X. Duan, J. K. Harper, F. J. Uribe-Romo, *J. Am. Chem. Soc.* **2016**, *138*, 9767.

[62] S.-T. Yang, J. Kim, H.-Y. Cho, S. Kim, W.-S. Ahn, *RSC Adv.* **2012**, *2*, 10179.

[63] J. Yoo, S.-J. Cho, G. Y. Jung, S. H. Kim, K.-H. Choi, J.-H. Kim, C. K. Lee, S. K. Kwak, S.-Y. Lee, *Nano Lett.* **2016**, *16*, 3292.

[64] D. D. Medina, J. M. Rotter, Y. Hu, M. Dogru, V. Werner, F. Auras, J. T. Markiewicz, P. Knochel, T. Bein, *J. Am. Chem. Soc.* **2015**, *137*, 1016.

[65] W. Huang, Y. Jiang, X. Li, X. Li, J. Wang, Q. Wu, X. Liu, *ACS Appl. Mater. Interfaces* **2013**, *5*, 8845.

[66] B. J. Smith, L. R. Parent, A. C. Overholts, P. A. Beaucage, R. P. Bisbey, A. D. Chavez, N. Hwang, C. Park, A. M. Evans, N. C. Gianneschi, W. R. Dichtel, *ACS Cent. Sci.* **2017**, *3*, 58.

[67] R. L. Li, N. C. Flanders, A. M. Evans, W. Ji, I. Castano, L. X. Chen, N. C. Gianneschi, W. R. Dichtel, *Chem. Sci.* **2019**, *10*, 3796.

[68] a) A. de la Peña Ruigómez, D. Rodríguez-San-Miguel, K. C. Stylianou, M. Cavallini, D. Gentili, F. Liscio, S. Milita, O. M. Roscioni, M. L. Ruiz-González, C. Carbonell, D. Maspoch, R. Mas-Ballesté, J. L. Segura, F. Zamora, *Chem. - Eur. J.* **2015**, *21*, 10666; b) D. Rodríguez-San-Miguel, A. Abrishamkar, J. A. R. Navarro,

R. Rodriguez-Trujillo, D. B. Amabilino, R. Mas-Ballesté, F. Zamora, J. Puigmartí-Luis, *Chem. Commun.* **2016**, *52*, 9212; c) D. Rodríguez-San-Miguel, J. J. Corral-Pérez, E. Gil-González, D. Cuellas, J. Arauzo, V. M. Monsalvo, V. Carcelén, F. Zamora, *CrystEngComm* **2017**, *19*, 4872.

[69] Y. Zhao, L. Guo, F. Gándara, Y. Ma, Z. Liu, C. Zhu, H. Lyu, C. A. Trickett, E. A. Kapustin, O. Terasaki, O. M. Yaghi, *J. Am. Chem. Soc.* **2017**, *139*, 13166.

[70] Q. Guan, D.-D. Fu, Y.-A. Li, X.-M. Kong, Z.-Y. Wei, W.-Y. Li, S.-J. Zhang, Y.-B. Dong, *iScience* **2019**, *14*, 180.

[71] J. Tan, S. Namuangruk, W. Kong, N. Kungwan, J. Guo, C. Wang, *Angew. Chem., Int. Ed.* **2016**, *55*, 13979.

[72] I. Berlanga, M. L. Ruiz-González, J. M. González-Calbet, J. L. G. Fierro, R. Mas-Ballesté, F. Zamora, *Small* **2011**, *7*, 1207.

[73] N. Keller, D. Bessinger, S. Reuter, M. Calik, L. Ascherl, F. C. Hanusch, F. Auras, T. Bein, *J. Am. Chem. Soc.* **2017**, *139*, 8194.

[74] D. N. Bunck, W. R. Dichtel, *J. Am. Chem. Soc.* **2013**, *135*, 14952.

[75] Y. Peng, Y. Huang, Y. Zhu, B. Chen, L. Wang, Z. Lai, Z. Zhang, M. Zhao, C. Tan, N. Yang, F. Shao, Y. Han, H. Zhang, *J. Am. Chem. Soc.* **2017**, *139*, 8698.

[76] C. Zhang, S. Zhang, Y. Yan, F. Xia, A. Huang, Y. Xian, *ACS Appl. Mater. Interfaces* **2017**, *9*, 13415.

[77] S. Wang, Q. Wang, P. Shao, Y. Han, X. Gao, L. Ma, S. Yuan, X. Ma, J. Zhou, X. Feng, B. Wang, *J. Am. Chem. Soc.* **2017**, *139*, 4258.

[78] a) Z. Kahveci, T. Islamoglu, G. A. Shar, R. Ding, H. M. El-Kaderi, *CrystEngComm* **2013**, *15*, 1524; b) T.-Y. Zhou, F. Lin, Z.-T. Li, X. Zhao, *Macromolecules* **2013**, *46*, 7745.

[79] a) S. Wan, J. Guo, J. Kim, H. Ihee, D. Jiang, *Angew. Chem., Int. Ed.* **2008**, *47*, 8826; b) S. Wan, J. Guo, J. Kim, H. Ihee, D. Jiang, *Angew. Chem., Int. Ed.* **2009**, *48*, 5439; c) E. L. Spitler, W. R. Dichtel, *Nat. Chem.* **2010**, *2*, 672; d) S. Kim, C. Park, M. Lee, I. Song, J. Kim, M. Lee, J. Jung, Y. Kim, H. Lim, H. C. Choi, *Adv. Funct. Mater.* **2017**, *27*, 1700925; e) B. Gole, V. Stepanenko, S. Rager, M. Grüne, D. D. Medina, T. Bein, F. Würthner, F. Beuerle, *Angew. Chem., Int. Ed.* **2018**, *57*, 846.

[80] S. Kandambeth, V. Venkatesh, D. B. Shinde, S. Kumari, A. Halder, S. Verma, R. Banerjee, *Nat. Commun.* **2015**, *6*, 6786.

[81] Z.-J. Yin, S.-Q. Xu, T.-G. Zhan, Q.-Y. Qi, Z.-Q. Wu, X. Zhao, *Chem. Commun.* **2017**, *53*, 7266.

[82] a) A. P. Côté, H. M. El-Kaderi, H. Furukawa, J. R. Hunt, O. M. Yaghi, *J. Am. Chem. Soc.* **2007**, *129*, 12914; b) S.-B. Yu, H. Lyu, J. Tian, H. Wang, D.-W. Zhang, Y. Liu, Z.-T. Li, *Polym. Chem.* **2016**, *7*, 3392.

[83] A. Nagai, Z. Guo, X. Feng, S. Jin, X. Chen, X. Ding, D. Jiang, *Nat. Commun.* **2011**, *2*, 536.

[84] N. Huang, R. Krishna, D. Jiang, *J. Am. Chem. Soc.* **2015**, *137*, 7079.

[85] L. Chen, K. Furukawa, J. Gao, A. Nagai, T. Nakamura, Y. Dong, D. Jiang, *J. Am. Chem. Soc.* **2014**, *136*, 9806.

[86] F. Xu, H. Xu, X. Chen, D. Wu, Y. Wu, H. Liu, C. Gu, R. Fu, D. Jiang, *Angew. Chem., Int. Ed.* **2015**, *54*, 6814.

[87] H. Xu, X. Chen, J. Gao, J. Lin, M. Addicoat, S. Irle, D. Jiang, *Chem. Commun.* **2014**, *50*, 1292.

[88] Q. Sun, B. Aguila, J. Perman, L. D. Earl, C. W. Abney, Y. Cheng, H. Wei, N. Nguyen, L. Wojtas, S. Ma, *J. Am. Chem. Soc.* **2017**, *139*, 2786.

[89] a) S. Chandra, T. Kundu, S. Kandambeth, R. BabaRao, Y. Marathe, S. M. Kunjir, R. Banerjee, *J. Am. Chem. Soc.* **2014**, *136*, 6570; b) C. Liu, W. Zhang, Q. Zeng, S. Lei, *Chem. - Eur. J.* **2016**, *22*, 6768; c) J. Zhang, L. Wang, N. Li, J. Liu, W. Zhang, Z. Zhang, N. Zhou, X. Zhu, *CrystEngComm* **2014**, *16*, 6547.

[90] N. Huang, X. Ding, J. Kim, H. Ihee, D. Jiang, *Angew. Chem., Int. Ed.* **2015**, *54*, 8704.

[91] a) X. Feng, L. Liu, Y. Honsho, A. Saeki, S. Seki, S. Irle, Y. Dong, A. Nagai, D. Jiang, *Angew. Chem., Int. Ed.* **2012**, *51*, 2618; b) X. Ding, J. Guo, X. Feng, Y. Honsho, J. Guo, S. Seki, P. Maitarad, A. Saeki, S. Nagase, D. Jiang, *Angew. Chem., Int. Ed.* **2011**, *50*, 1289.

[92] a) S. Jin, X. Ding, X. Feng, M. Supur, K. Furukawa, S. Takahashi, M. Addicoat, M. E. El-Khouly, T. Nakamura, S. Irle, S. Fukuzumi,

**ADVANCED
SCIENCE NEWS**

www.advancedsciencenews.com

**ADVANCED
FUNCTIONAL
MATERIALS**

www.afm-journal.de

A. Nagai, D. Jiang, *Angew. Chem., Int. Ed.* **2013**, *52*, 2017; b) S. Jin, M. Supur, M. Addicoat, K. Furukawa, L. Chen, T. Nakamura, S. Fukuzumi, S. Irle, D. Jiang, *J. Am. Chem. Soc.* **2015**, *137*, 7817.

[93] X. Ding, X. Feng, A. Saeki, S. Seki, A. Nagai, D. Jiang, *Chem. Commun.* **2012**, *48*, 8952.

[94] a) D. Cao, J. Lan, W. Wang, B. Smit, *Angew. Chem., Int. Ed.* **2009**, *48*, 4730; b) J.-H. Guo, H. Zhang, Y. Miyamoto, *Phys. Chem. Chem. Phys.* **2013**, *15*, 8199; c) M. M. Wu, Q. Wang, Q. Sun, P. Jena, Y. Kawazoe, *J. Chem. Phys.* **2010**, *133*, 154706; d) J. Lan, D. Cao, W. Wang, B. Smit, *ACS Nano* **2010**, *4*, 4225.

[95] a) S. Yamaguchi, K. Kamiya, K. Hashimoto, S. Nakanishi, *Chem. Commun.* **2017**, *53*, 10437; b) X. Han, Q. Xia, J. Huang, Y. Liu, C. Tan, Y. Cui, *J. Am. Chem. Soc.* **2017**, *139*, 8693.

[96] S. Lin, C. S. Diercks, Y.-B. Zhang, N. Kornienko, E. M. Nichols, Y. Zhao, A. R. Paris, D. Kim, P. Yang, O. M. Yaghi, C. J. Chang, *Science* **2015**, *349*, 1208.

[97] W. Zhang, P. Jiang, Y. Wang, J. Zhang, Y. Gao, P. Zhang, *RSC Adv.* **2014**, *4*, 51544.

[98] X. Chen, N. Huang, J. Gao, H. Xu, F. Xu, D. Jiang, *Chem. Commun.* **2014**, *50*, 6161.

[99] H. B. Aiyappa, J. Thote, D. B. Shinde, R. Banerjee, S. Kurungot, *Chem. Mater.* **2016**, *28*, 4375.

[100] M. Calik, T. Sick, M. Dogru, M. Döblinger, S. Datz, H. Budde, A. Hartschuh, F. Auras, T. Bein, *J. Am. Chem. Soc.* **2016**, *138*, 1234.

[101] a) G. Gregoriadis, *N. Engl. J. Med.* **1976**, *295*, 704; b) H. Deng, K. Song, X. Zhao, Y. Li, F. Wang, J. Zhang, A. Dong, Z. Qin, *ACS Appl. Mater. Interfaces* **2017**, *9*, 9315; c) S. Bhunia, V. Radha, A. Chaudhuri, *Nanoscale* **2017**, *9*, 1201; d) B. S. Pattni, V. V. Chupin, V. P. Torchilin, *Chem. Rev.* **2015**, *115*, 10938; e) W. T. Al-Jamal, K. Kostarelos, *Acc. Chem. Res.* **2011**, *44*, 1094.

[102] a) K. E. Uhrich, S. M. Cannizzaro, R. S. Langer, K. M. Shakesheff, *Chem. Rev.* **1999**, *99*, 3181; b) J. Gong, M. Chen, Y. Zheng, S. Wang, Y. Wang, *J. Controlled Release* **2012**, *159*, 312; c) K. S. Soppimath, T. M. Aminabhavi, A. R. Kulkarni, W. E. Rudzinski, *J. Controlled Release* **2001**, *70*, 1; d) E. R. Gillies, J. M. J. Fréchet, *Drug Discovery Today* **2005**, *10*, 35; e) Y. Shamay, M. Elkabets, H. Li, J. Shah, S. Brook, F. Wang, K. Adler, E. Baut, M. Scaltriti, P. V. Jena, E. E. Gardner, J. T. Poirier, C. M. Rudin, J. Baselga, A. Haimovitz-Friedman, D. A. Heller, *Sci. Transl. Med.* **2016**, *8*, 345ra87.

[103] a) H. Yuan, K. Luo, Y. Lai, Y. Pu, B. He, G. Wang, Y. Wu, Z. Gu, *Mol. Pharmaceutics* **2010**, *7*, 953; b) B. K. Nanjwade, H. M. Bechra, G. K. Derkar, F. V. Manvi, V. K. Nanjwade, *Eur. J. Pharm. Sci.* **2009**, *38*, 185.

[104] a) D. Bitounis, H. Ali-Boucetta, B. H. Hong, D.-H. Min, K. Kostarelos, *Adv. Mater.* **2013**, *25*, 2258; b) G. Reina, J. M. González-Domínguez, A. Criado, E. Vázquez, A. Bianco, M. Prato, *Chem. Soc. Rev.* **2017**, *46*, 4400; c) R. Alshehri, A. M. Ilyas, A. Hasan, A. Arnaout, F. Ahmed, A. Memic, *J. Med. Chem.* **2016**, *59*, 8149; d) M. Lamberti, P. Pedata, N. Sannolo, S. Porto, A. De Rosa, M. Caraglia, *Int. J. Immunopathol. Pharmacol.* **2015**, *28*, 4.

[105] a) H. Tomás, C. S. Alves, J. Rodrigues, *Nanomed.: Nanotechnol., Biol. Med.* **2018**, *14*, 2407; b) A. K. Gaharwar, S. M. Mihaila, A. Swami, A. Patel, S. Sant, R. L. Reis, A. P. Marques, M. E. Gomes, A. Khademhosseini, *Adv. Mater.* **2013**, *25*, 3329.

[106] a) I. I. Slowing, B. G. Trewyn, V. S. Y. Lin, *J. Am. Chem. Soc.* **2007**, *129*, 8845; b) A. Watermann, J. Brieger, *Nanomaterials* **2017**, 7, 189.

[107] a) T. Yadavalli, D. Shukla, *Nanomed.: Nanotechnol., Biol. Med.* **2017**, *13*, 219; b) Q. Quan, J. Xie, H. Gao, M. Yang, F. Zhang, G. Liu, X. Lin, A. Wang, H. S. Eden, S. Lee, G. Zhang, X. Chen, *Mol. Pharmaceutics* **2011**, *8*, 1669; c) K. Ulbrich, K. Holá, V. Šubr, A. Bakandritsos, J. Tuček, R. Zbořil, *Chem. Rev.* **2016**, *116*, 5338.

[108] a) J. Shi, P. W. Kantoff, R. Wooster, O. C. Farokhzad, *Nat. Rev. Cancer* **2017**, *17*, 20; b) D. Bobo, K. J. Robinson, J. Islam, K. J. Thurecht, S. R. Corrie, *Pharm. Res.* **2016**, *33*, 2373.

[109] a) F. X. Gu, R. Karnik, A. Z. Wang, F. Alexis, E. Levy-Nissenbaum, S. Hong, R. S. Langer, O. C. Farokhzad, *Nano Today* **2007**, *2*, 14; b) P. Majumder, S. Bhunia, J. Bhattacharyya, A. Chaudhuri, *J. Controlled Release* **2014**, *180*, 100; c) N. Muhamad, T. Plengsuriyakarn, K. Na-Bangchang, *Int. J. Nanomed.* **2018**, *13*, 3921.

[110] a) H.-J. Li, J.-Z. Du, X.-J. Du, C.-F. Xu, C.-Y. Sun, H.-X. Wang, Z.-T. Cao, X.-Z. Yang, Y.-H. Zhu, S. Nie, J. Wang, *Proc. Natl. Acad. Sci. USA* **2016**, *113*, 4164; b) N. V. Rao, H. Ko, J. Lee, J. H. Park, *Front. Bioeng. Biotechnol.* **2018**, *6*, 110.

[111] L. Chen, J. Liu, Y. Zhang, G. Zhang, Y. Kang, A. Chen, X. Feng, L. Shao, *Nanomedicine* **2018**, *13*, 1939.

[112] a) M. J. Pallardy, I. Turbica, A. Biola-Vidamment, *Front. Immunol.* **2017**, *8*, 544; b) N. M. La-Beck, A. A. Gabizon, *Front. Immunol.* **2017**, 8, 416.

[113] L. Bai, S. Z. F. Phua, W. Q. Lim, A. Jana, Z. Luo, H. P. Tham, L. Zhao, Q. Gao, Y. Zhao, *Chem. Commun.* **2016**, *52*, 4128.

[114] V. S. Vyas, M. Vishwakarma, I. Moudrakovski, F. Haase, G. Savasci, C. Ochsenfeld, J. P. Spatz, B. V. Lotsch, *Adv. Mater.* **2016**, *28*, 8749.

[115] S. Kanti Das, S. Mishra, K. Manna, U. Kayal, S. Mahapatra, K. Das Saha, S. Dalapati, G. P. Das, A. A. Mostafa, A. Bhaumik, *Chem. Commun.* **2018**, *54*, 11475.

[116] G. Zhang, X. Li, Q. Liao, Y. Liu, K. Xi, W. Huang, X. Jia, *Nat. Commun.* **2018**, *9*, 2785.

[117] S. Gan, X. Tong, Y. Zhang, J. Wu, Y. Hu, A. Yuan, *Adv. Funct. Mater.* **2019**, *29*, 1902757.

[118] L. Zhang, S. Wang, Y. Zhou, C. Wang, X.-Z. Zhang, H. Deng, *Angew. Chem., Int. Ed.* **2019**, *58*, 14213.

[119] Y. Zhang, L. Zhang, Z. Wang, F. Wang, L. Kang, F. Cao, K. Dong, J. Ren, X. Qu, *Biomaterials* **2019**, *223*, 119462.

[120] Z. Mi, P. Yang, R. Wang, J. Unruangsri, W. Yang, C. Wang, J. Guo, *J. Am. Chem. Soc.* **2019**, *141*, 14433.

[121] K. Wang, Z. Zhang, L. Lin, K. Hao, J. Chen, H. Tian, X. Chen, *ACS Appl. Mater. Interfaces* **2019**, *11*, 39503.

[122] Q. Guan, L.-L. Zhou, Y.-A. Li, W.-Y. Li, S. Wang, C. Song, Y.-B. Dong, *ACS Nano* **2019**, *13*, 13304.

[123] C. Hu, Z. Zhang, S. Liu, X. Liu, M. Pang, *ACS Appl. Mater. Interfaces* **2019**, *11*, 23072.

[124] C. Hu, L. Cai, S. Liu, M. Pang, *Chem. Commun.* **2019**, *55*, 9164.

[125] D. Wang, Z. Zhang, L. Lin, F. Liu, Y. Wang, Z. Guo, Y. Li, H. Tian, X. Chen, *Biomaterials* **2019**, *223*, 119459.

[126] P. Wang, M. Kang, S. Sun, Q. Liu, Z. Zhang, S. Fang, *Chin. J. Chem.* **2014**, *32*, 838.

[127] X. Yan, Y. Song, J. Liu, N. Zhou, C. Zhang, L. He, Z. Zhang, Z. Liu, *Biosens. Bioelectron.* **2019**, *126*, 734.

[128] M. Wang, M. Hu, J. Liu, C. Guo, D. Peng, Q. Jia, L. He, Z. Zhang, M. Du, *Biosens. Bioelectron.* **2019**, *132*, 8.

[129] X. Liu, M. Hu, M. Wang, Y. Song, N. Zhou, L. He, Z. Zhang, *Biosens. Bioelectron.* **2019**, *123*, 59.

[130] R. M. Dirks, N. A. Pierce, *Proc. Natl. Acad. Sci. USA* **2004**, *101*, 15275.

[131] W. Li, C.-X. Yang, X.-P. Yan, *Chem. Commun.* **2017**, *53*, 11469.

[132] G. Das, F. Benyettou, S. K. Sharama, T. Prakasam, F. Gándara, V. A. de la Peña-O'Shea, N. Saleh, R. Pasricha, R. Jagannathan, M. A. Olson, A. Trabolsi, *Chem. Sci.* **2018**, *9*, 8382.

[133] P. Wang, F. Zhou, C. Zhang, S.-Y. Yin, L. Teng, L. Chen, X.-X. Hu, H.-W. Liu, X. Yin, X.-B. Zhang, *Chem. Sci.* **2018**, *9*, 8402.

[134] Q. Sun, C.-W. Fu, B. Aguila, J. Perman, S. Wang, H.-Y. Huang, F.-S. Xiao, S. Ma, *J. Am. Chem. Soc.* **2018**, *140*, 984.

[135] Q. Sun, B. Aguila, P. C. Lan, S. Ma, *Adv. Mater.* **2019**, *31*, 1900008.

[136] M. S. Lohse, T. Stassin, G. Naudin, S. Wuttke, R. Ameloot, D. De Vos, D. D. Medina, T. Bein, *Chem. Mater.* **2016**, *28*, 626.

[137] A. Samui, Happy, S. K. Sahu, *Microporous Mesoporous Mater.* **2020**, *291*, 109700.

[138] T. Liu, X. Hu, Y. Wang, L. Meng, Y. Zhou, J. Zhang, M. Chen, X. Zhang, *J. Photochem. Photobiol., B* **2017**, *175*, 156.